iScience

CellPress
OPEN ACCESS

Article

Modulation of social investigation by anterior hypothalamic nucleus rhythmic neural activity

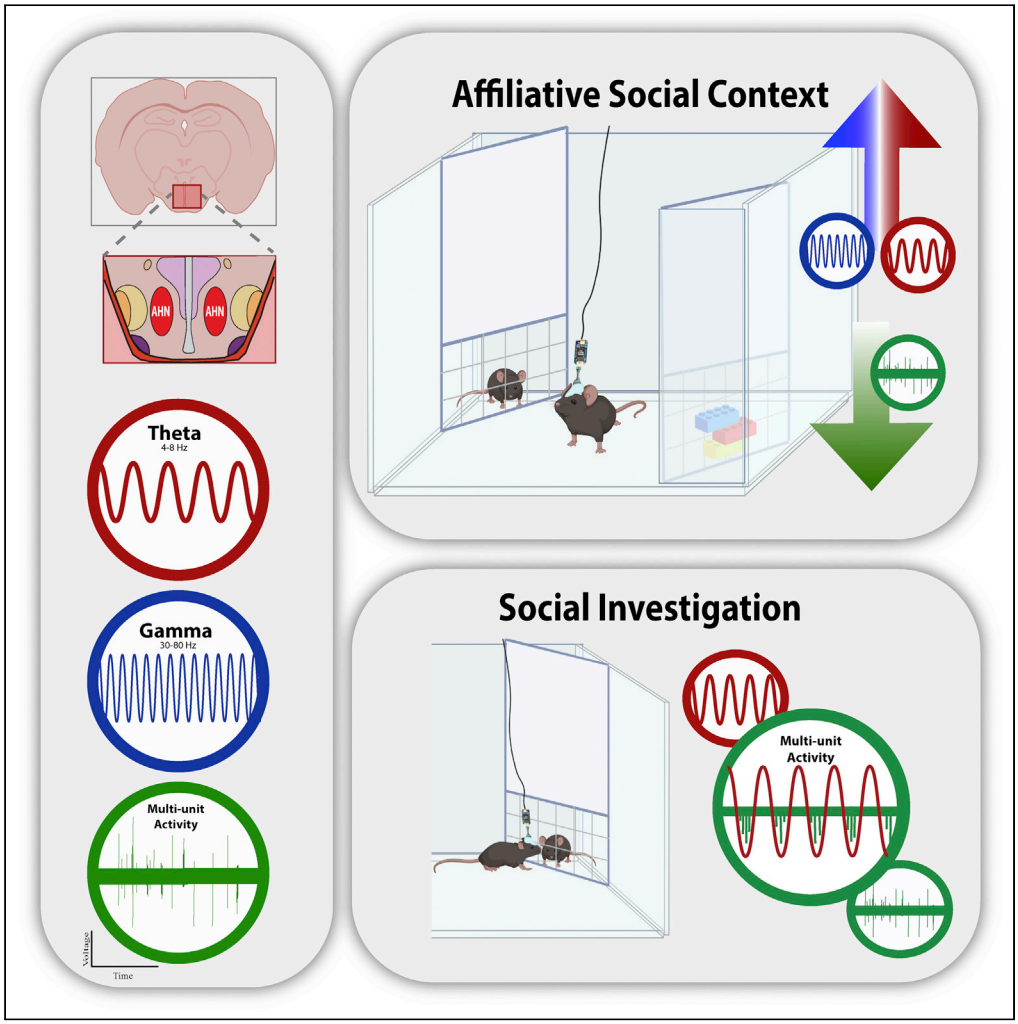

Renad Jabarin, Wael Dagash, Shai Netser, Shelly Singh, Blesson K. Paul, Edi Barkai, Shlomo Wagner

shlomow@research.haifa.ac.il

Highlights

Affiliative, but not aversive social interactions enhance AHN LFP theta rhythmicity

AHN spiking activity increases during the investigation of social stimuli

AHN spiking activity shows theta modulation during the investigation of social stimuli

AHN optogenetic stimulation during social interactions augments approach behavior

Jabarin et al., iScience 26, 105921
February 17, 2023
https://doi.org/10.1016/j.isci.2022.105921

iScience

CellPress
OPEN ACCESS

Article

Modulation of social investigation by anterior hypothalamic nucleus rhythmic neural activity

Renad Jabarin,[1,2] Wael Dagash,[1,2] Shai Netser,[1,2] Shelly Singh,[1] Blesson K. Paul,[1] Edi Barkai,[1] and Shlomo Wagner[1,3,*]

SUMMARY

Social interactions involve both approach and avoidance toward specific individuals. Currently, the brain regions subserving these behaviors are not fully recognized. The anterior hypothalamic nucleus (AHN) is a poorly defined brain area, and recent studies have yielded contradicting conclusions regarding its behavioral role. Here we explored the role of AHN neuronal activity in regulating approach and avoidance actions during social interactions. Using electrophysiological recordings from behaving mice, we revealed that theta rhythmicity in the AHN is enhanced during affiliative interactions, but decreases during aversive ones. Moreover, the spiking activity of AHN neurons increased during the investigation of social stimuli, as compared to objects, and was modulated by theta rhythmicity. Finally, AHN optogenetic stimulation during social interactions augmented the approach toward stimuli associated with the stimulation. These results suggest the role for AHN neural activity in regulating approach behavior during social interactions, and for theta rhythmicity in mediating the valence of social stimuli.

INTRODUCTION

Social interactions are highly complex, involving both approach and avoidance actions toward specific individuals. Thus, in a certain social context, a subject may approach one individual (a friend) while avoiding a second one (a foe). Moreover, the same type of behavior may be driven by distinct intentions, such that a subject may approach an individual in either an affiliative or an offensive manner. These characteristics make the neurobiological mechanisms underlying social behavior difficult to elucidate.[1] Nevertheless, during the last two decades, a plethora of studies have begun to reveal brain circuits subserving various types of social behavior for recent reviews see for example.[2–9] These studies revealed the involvement of a vast network of mostly limbic brain regions, termed the social behavior network (SBN), in regulating mammalian social behavior.[10,11] Several of these regions reside in the hypothalamus, a brain structure known to control innate social behaviors, such as mating, aggression, and parenting.[5,12–14] However, it is likely that additional brain regions are involved in regulating social behavior.

One such brain region with a potential role in regulating social interactions is the anterior hypothalamic nucleus (AHN, also known as the anterior hypothalamic area - AHA). The AHN is a relatively understudied and poorly defined brain area, known as part of the medial hypothalamic defensive system.[15] It includes mainly inhibitory GABAergic neurons[16–18] which largely project to several brain regions thought to be central to fight-or-flight behavior, such as the lateral septum (LS) and dorsal periaqueductal gray (dPAG) area.[18,19] In rats and mice, the AHN was shown to take part in responses to predators[20–22] as well as in regulating parental behavior.[23] In recent years, several studies explored the role of AHN neurons in the context of anxiety and avoidance behaviors, using advanced techniques (e.g., optogenetics), with contradictory results.[16,17,24] Yet, none of these studies examined the role of the AHN in the context of social behavior. Another recent study (Xie et al. 2021) demonstrated that vGAT-positive cells, a population consisting of about 90% of AHN neurons, are involved in attack behavior that follows physical noxious stimuli. Such an attack may be considered the opposite response to escape, as it requires approaching the threat rather than avoiding it. Intriguingly, this study reported that in a social setting, optogenetic activation of GABAergic AHN neurons reduces aggression and enhances social investigation. These results suggest that the behavioral contribution of the AHN is context-dependent and that it's role differs in the affiliative social context than in other contexts such as during predator's attack.

[1]Sagol Department of Neurobiology, the Integrated Brain and Behavior Research Center (IBBRC), University of Haifa, Mt. Carmel, Haifa 3498838, Israel

[2]These authors contributed equally

[3]Lead contact

*Correspondence: shlomow@research.haifa.ac.il

https://doi.org/10.1016/j.isci.2022.105921

Here we hypothesize that in social contexts AHN activity modulates approach behavior toward specific stimuli. To unravel the behavioral contribution of the AHN in social contexts, we explored the role of AHN neurons in regulating approach and avoidance actions toward distinct stimuli during social discrimination tasks. To that end, we used electrophysiological recording of neuronal population activity in the AHN, c-Fos staining, and direct optogenetic stimulation. We found that theta rhythmicity in the AHN was enhanced during affiliative, but decreased during aversive social interactions and that the level of spiking activity of AHN neurons was higher during the investigation of social stimuli, as compared to objects. Notably, the spiking activity of AHN neurons was found to be modulated by LFP theta rhythmicity during social interactions. Finally, we found that during social interaction, direct optogenetic stimulation of AHN neurons modulated approach behavior toward stimuli associated with this stimulation. Overall, our results suggest a role for AHN neural activity in regulating approach behavior during social interactions, and for theta rhythmicity in mediating the valence of the social context.

RESULTS

Theta and gamma power of local field potential in the anterior hypothalamic nucleus increase during social interaction

For recording neural activity from the AHN of behaving mice (n = 17 adult male mice), we chronically implanted tetrodes (4 × 4; Figure S1A) in this brain area and conducted behavioral experiments, while recording electrophysiological signals. Each experiment comprised a 5-min social preference (SP) session (Figures 1A and 1B), followed 30 min later by a 5-min session of free social interactions (Figures S2A and S2B). For each electrophysiological recording, we separately analyzed local field potential signals (LFP; low-pass filtered at 0.3 kHz) and spiking activity (band-pass filtered at 0.3-5 kHz). LFP signals were analyzed first by generating a power spectral density (PSD) profile separately for each of the three 5-min stages of the session: Pre-encounter, Encounter, and Post-encounter. As apparent in the single-session example displayed in Figure 1C, while the Pre-encounter and Post-encounter profiles were almost identical, the Encounter profile reflected increased power in both the theta (4-10 Hz) and gamma (30-80 Hz) bands, suggesting enhanced theta and gamma rhythmicity in the AHN during social interaction.

We analyzed the behavior of the subjects during the SP task using our published automated analysis system.[25] This system allows precise tracking of investigation bouts conducted by the subject mouse toward each of two chambers containing either a novel conspecific (social stimulus) or an object.[26] As apparent in Figures 1D–1F, while the subjects did not prefer any of the empty chambers in the Pre-encounter stage, they showed a clear preference for investigating the chamber of the social stimulus during the Encounter stage (Paired t-test: $t_{41} = 10.152$, $p < 0.001$). At the Post-encounter stage, for a while, the subjects kept a preference for the empty chamber that previously contained the social stimulus. This preference gradually disappeared.

We used *Z* score analysis to normalize the theta and gamma power of the LFP signals recorded during the various experiments, with the Pre-encounter stage serving as a baseline (Figures 1G–1J). We found a clear increase in both theta and gamma power following the introduction of the social stimulus to the arena, compared to the Pre-encounter stage (Figures 1G–1J). This increase was statistically significant for both the first 2 min and last 2 min of the session. Similar results were observed for the same variables recorded from the same animals during free social interactions (Figures S2E–S2H).

As theta rhythmicity in the hippocampus is known to be associated with the subject's movement, we examined the relation between AHN theta rhythmicity and the subject's movement, separately for the various stages of the SP test. We found a significantly higher mean speed during the Encounter stage as compared to Pre-encounter, and this elevated speed was not reduced during the Post-encounter stage (Figure S3A). In contrast, the theta power was significantly reduced during the Post-encounter stage as compared to Encounter (Figure S3B). Given that analysis of covariance revealed a similar relationship between LFP theta power and the subject's speed across all three stages of the test (Figure S3C), we conclude that the subject's movement may contribute to, but not fully explain the increase in AHN theta power during the social encounter.

Spiking activity in the anterior hypothalamic nucleus is generally reduced but gets more rhythmic during social interactions

For analyzing the spiking activity recorded during the SP and free interaction experiments (shown in Figures 1 and S2, respectively), this activity was sorted into single- and multi-units (SUA and MUA, respectively; Figures S1B and S1D). Notably, since we managed to reliably separate only a relatively low number of SUAs

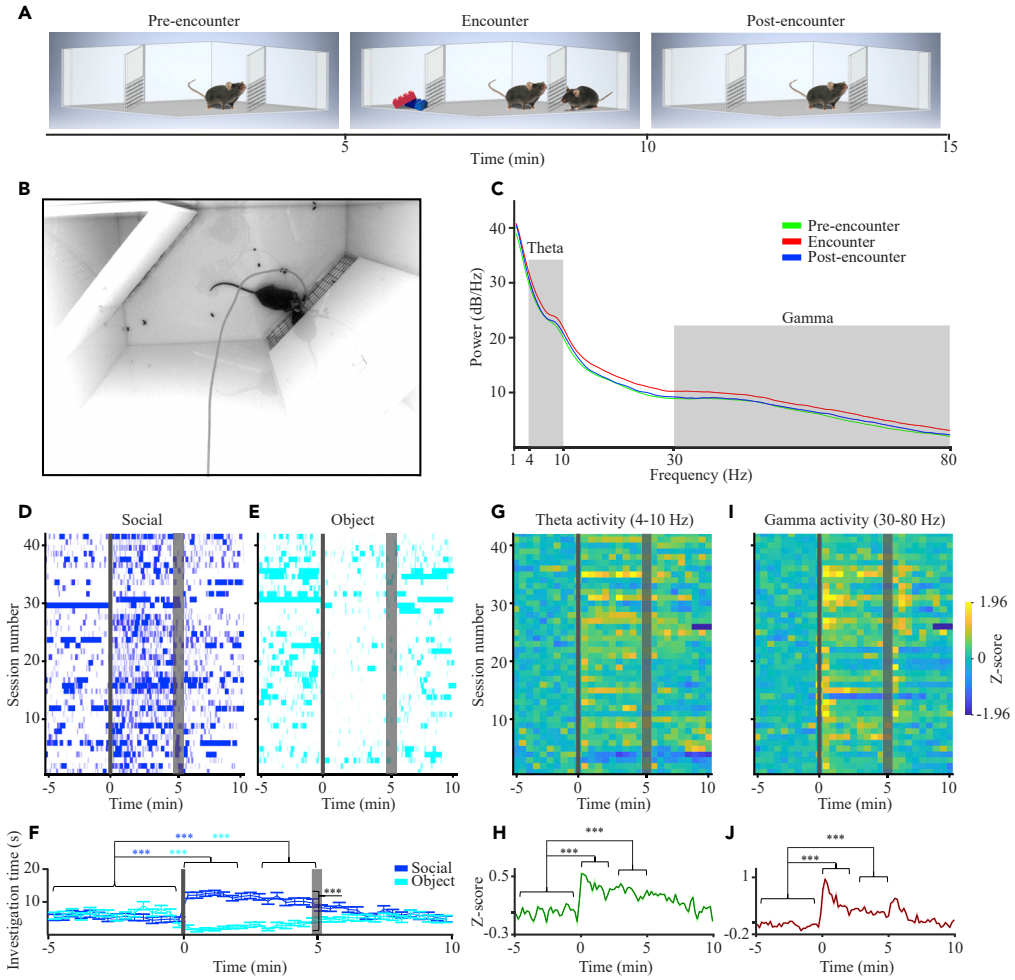

Figure 1. AHN theta and gamma rhythms are enhanced during the social preference (SP) test

(A) Schematic depiction of the three stages of the SP test.

(B) A picture of the experimental arena during the SP test.

(C) Power spectral density (PSD) profiles of local field potential (LFP) signals recorded during each of the three 5-min stages of the test from a single animal, color-coded according to the test stage. The theta (4-10 Hz) and Gamma (30-80 Hz) ranges are labeled in gray.

(D) Behavioral raster-plots of investigation bouts toward social stimuli along 42 sessions. Gray bars represent the time of insertion (thin bar) and removal (thick bar) of the stimuli from the chambers. Time 0 represents the beginning of the test.

(E) As in D, for object stimuli during the same sessions.

(F) Mean investigation time (±SEM, 20-s bins) during the same sessions shown in D-E, plotted separately for the social (blue) and object (light blue) stimuli. Note the statistically significant change from the 5-min Baseline, in investigation time of both social (increase) and object (decrease) stimuli during the first and last 2 min of the Encounter. Significant main effects were found in 2-way repeated measures (RM) ANOVA for Time ($p<0.01$), Stimulus ($p<0.001$) and Time × Stimulus interaction ($p < 0.001$) effects.

(G) Heatmap of *Z* score analysis of theta power of LFP signals recorded during the same sessions shown in D-E.

(H) Mean (±SEM) *Z* score analysis of theta power of LFP signals recorded during the same sessions shown in D-E. Significant main effect for Time was found in RM ANOVA($p < 0.001$).

(I) As in F, for gamma power.

(J) As in H, for gamma power. Significant main effect for Time was found in RM ANOVA($p < 0.001$). ***$p < 0.001$, paired t-test with Bonferroni correction for multiple comparisons following main effects in ANOVA. See also Figures S2 and S3.

(2 out of 34 for SP and 33 out of 89 for free interaction), we pooled all SUAs and MUAs together and considered them all as MUAs. As apparent in Figure S1E, while analyzing the firing rate across each session, we observed variable responses of these MUAs. For example, some MUAs responded to the social stimulus insertion with increased activity (Figure S1E, first trace), some responded with transient inhibition (second

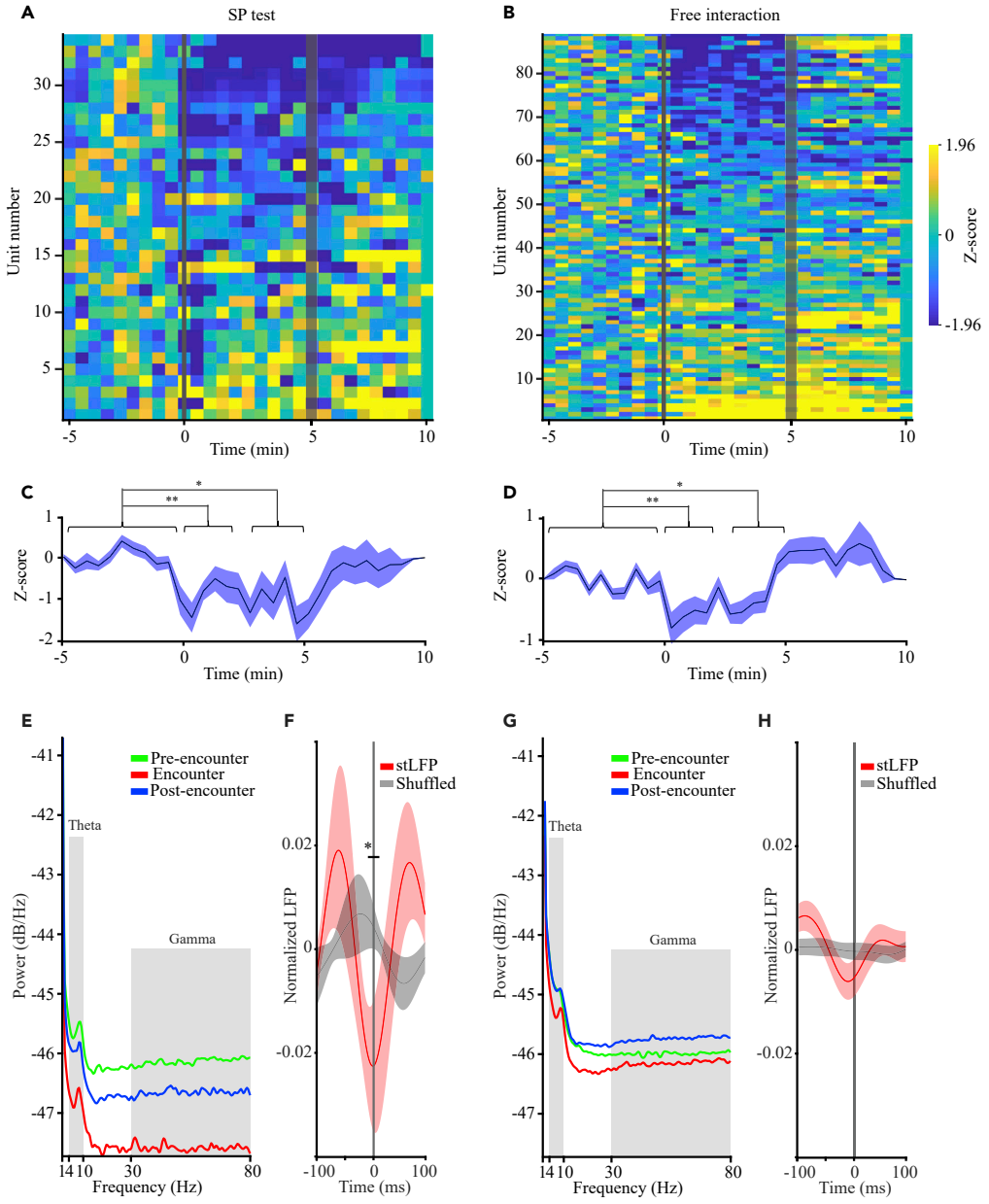

Figure 2. AHN Spiking activity is generally reduced and synchronizes with the LFP theta rhythm during the social encounter

(A) Heat-maps of *Z* score analysis of multi-unit activity (MUA) for all units recorded during SP tests, sorted from inhibition (top) to excitation (bottom).

(B) As in A, for free interaction sessions.

(C) Mean (±SEM) *Z* score analysis of the units shown in A. Note the statistically significant decrease in mean spiking activity during the first (left) and last (right) 2 min of the Encounter, as compared to the 5-min Baseline stage. Significant main effect for Time was found in RM ANOVA($p < 0.01$).

(D) As in C, for the units shown in B. Significant main effect for Time was found in RM ANOVA($p < 0.001$).

(E) PSD profiles of the MUA recorded during each stage of the SP test, color-coded according to the test stage. The theta and gamma ranges are labeled in gray. Note the general reduction during the Encounter stage, which is caused by the lower mean firing rate at this stage, as compared to the other stages. Also, note the clear peak at the theta range, demonstrating theta rhythmicity of spiking activity.

(F) Spike-triggered LFP (stLFP, ±SEM) of theta-filtered LFP signals (red) and of shuffled LFP signals (gray) for the Encounter period. Note the statistically significant difference between the mean stLFP and shuffled signals at time

Figure 2. *Continued*

0 (between −10 and 10 ms), suggesting the synchronization of spiking activity and LFP theta rhythmicity. Significant difference was found in the paired t-test ($p < 0.05$).

(G) As in E, for free-interaction experiments.

(H) As in F, for free-interaction experiments. Note that here the difference between STA and shuffled signals is not statistically significant in the paired t-test ($p = 0.15$), but keeps the same trend as for the SP sessions shown in F. *$p < 0.05$, **$p < 0.01$, paired t-test with Bonferroni correction for multiple comparisons following main effects in ANOVA. See also Figure S1.

trace), some increased their activity only after stimulus removal (third trace) and some did not respond at all (fourth trace). This variability was also demonstrated by the heatmaps representing the *Z* score analysis of all MUAs recorded during SP (Figure 2A) and free interaction (Figure 2B) sessions. However, when the mean *Z* score of all MUAs was calculated, we observed a general inhibition in firing rate for both SP (Figure 2C) and free interaction (Figure 2D) sessions. This inhibition was statistically significant, compared to baseline, for both the first 2 min and last 2 min of both types of sessions. Thus, social interaction is accompanied by a general reduction in the firing rate of AHN neurons.

Despite the general reduction in spiking activity, it may be possible that during social interactions, when the power of LFP theta and gamma rhythmicity is high, spiking activity is synchronized by these rhythms to create more coherent firing of the neuronal population.[27] To examine this possibility, we first calculated the PSD profiles of the spiking activity for the various stages of the SP paradigm. While the general power was reduced during the encounter due to the general reduction in firing, a clear peak at the theta range was apparent, suggesting significant theta rhythmicity of spiking activity (Figure 2E). To examine possible synchronization between LFP theta rhythmicity and firing activity, we conducted spike-triggered LFP averaging (stLFP) of the theta-filtered LFP signals and compared it to shuffled signals. We found that during the Encounter period there was a significant difference between the stLFP and the shuffled LFP profile, suggesting preferred firing at the trough of the LFP theta rhythm (Figure 2F). Qualitatively similar results were obtained during free interaction sessions, although in this case the difference between the stLFP and the shuffled LFP profile was not statistically significant (Figures 2G and 2H). Overall, these results suggest synchronization between the firing activity and the LFP theta rhythmicity during the social encounter.

Anterior hypothalamic nucleus spiking activity correlates with stimulus investigation in a stimulus-dependent manner

Next, we examined each of the recorded variables (theta power, gamma power, and firing rate) in correlation with the specific investigation bouts, analyzed separately for each stimulus (object and social). Such an analysis can be done reliably only for SP sessions, while in free interaction sessions it is difficult to determine the exact starting point of each investigation bout. As for both theta and gamma power, while there seems to be a weak increase in the *Z* score in response to both types of stimuli during the first 2 s following the bout beginning, this increase was hardly significant and no significant difference was observed between bouts toward social and object stimuli [Figures 3A–3F]. In contrast, when MUA firing rate was analyzed using the same methodology, we found a statistically significant change, compared to the baseline, for social investigation bouts (Figures 3G–3I). Yet, while social investigation bouts were characterized by a significant increase in firing rate, investigation of object stimuli elicited an initial increase in *Z* score, followed by a significant decline 4-5 s after the beginning of the investigation bout. Consequently, a statistically significant difference between responses to social and object stimuli was observed 4-5 s after the beginning of the investigation bout (Figure 3I). To make sure that this difference is not due to the fact that a larger portion of object investigation bouts are shorter than 5 s, we compared the *Z* score of spiking activity between investigation bouts which are longer than 6 s (Figures S4A and S4B) and found that even in this comparison there was a highly significant difference between social and object investigation bouts at 4-5 s after the beginning of the bout (Figure S4C). Altogether, these results suggest that while theta or gamma rhythms in the AHN are related to the social context, and therefore show a general increase during social interaction, spiking activity correlates with stimulus investigation, in a stimulus-dependent manner.

Anterior hypothalamic nucleus theta rhythmicity of local field potential signals differs between attractive and aversive social stimuli

So far, we have explored AHN activity during interactions of the subject animals with stimuli that are both attractive, although at different levels of attractiveness (social vs. object stimuli). Yet, avoidance behavior is usually exhibited toward aversive stimuli. Thus, it may be that neural activity in the AHN differs between

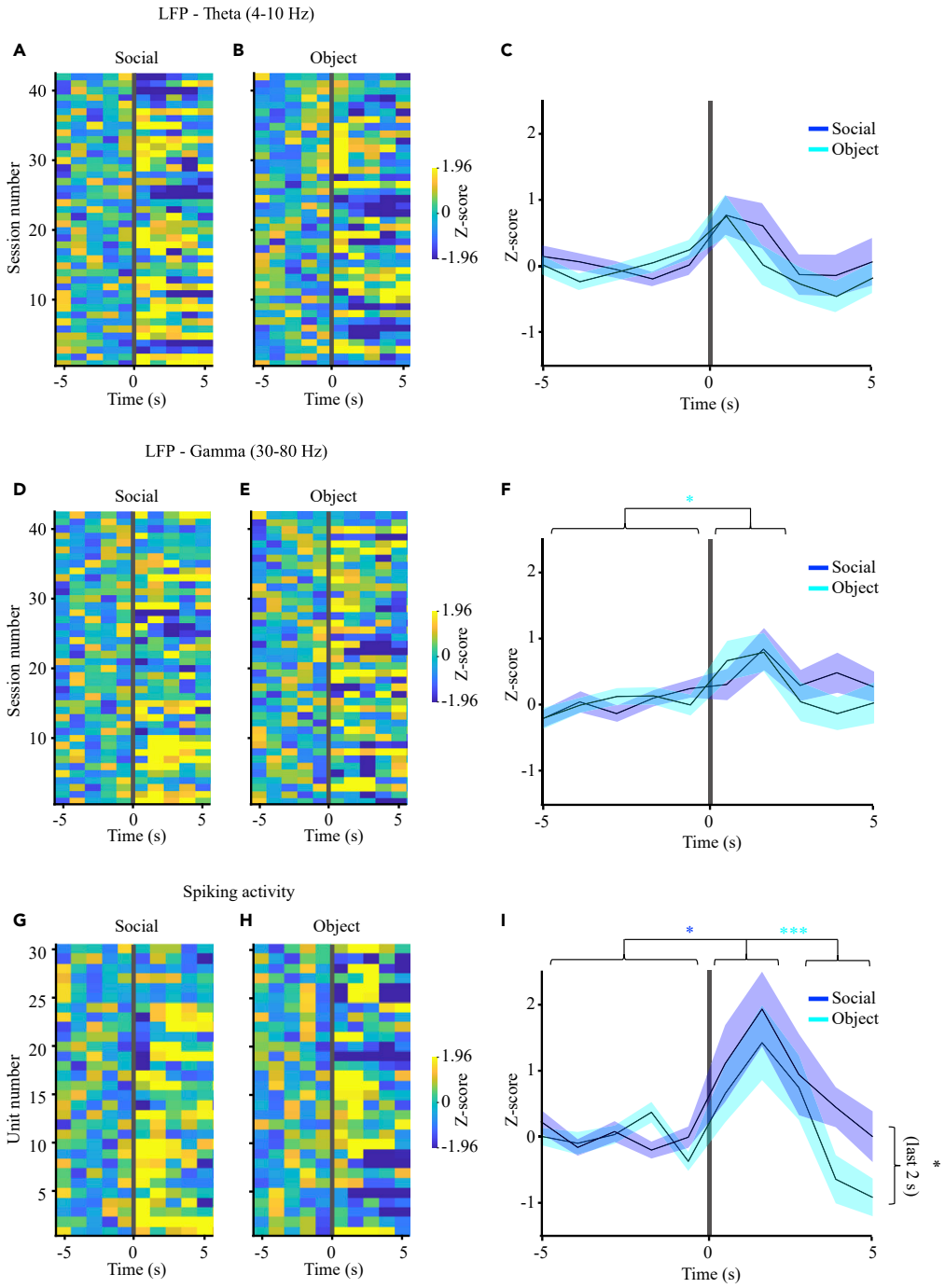

Figure 3. Spiking activity, but not LFP rhythms, is specifically enhanced during social investigation bouts

(A) Heat maps of mean *Z* score of LFP theta power recorder from 5-s before to 5-s after the beginning of social investigation during SP sessions. Each line represents the mean value averaged across all bouts for a single session.

(B) As in A, for object investigation bouts during the same sessions.

(C) Mean (±SEM) *Z* score analysis for all the sessions shown in A-B, averaged separately for social (blue) and object (light blue) stimuli. Significant main effect for Time was found in 2-way RM ANOVA($p < 0.01$). However, no significant post hoc changes were found, as compared to the baseline (5 s before beginning of bout) period.

(D) As in A, for gamma power.

(E) As in B, for gamma power.

Figure 3. *Continued*

(F) As in C, for gamma power. Significant main effect for Time was found in 2-way RM ANOVA($p < 0.01$). Note that in this case a slightly significant increase was observed for the first 2 s of the bout toward the object stimulus, as compared to the baseline.

(G) As in A, for MUA.

(H) As in B, for MUA.

(I) As in C, for MUA. Significant main effect for Time was found in 2-way RM ANOVA($p < 0.01$). Note that a significant change from baseline was found for social investigation during the first 2 s, while for object investigation the last 2 s were significantly lower than the first 2 s. Note also that a significant difference was observed between social and object investigation bouts during the last 2 s *$p < 0.05$, ***$p < 0.001$, paired t-test with Bonferroni correction for multiple comparisons following the main effect in ANOVA.

attractive and aversive stimuli. To examine this possibility in a social context, we employed a stimulus-specific social fear conditioning (SFC) paradigm (schematically described in Figure 4A and in more detail in Figure S5A), that compares between affiliative (CS^-) and aversive (CS^+) social stimuli. The CS^- and CS^+ stimuli were of different mouse strains (C57BL/6J and ICR), so as to enhance the ability of a subject to discriminate between them. First, each subject (n = 7 mice) performed two consecutive SP tests (Baseline tests, separated by 15 min) before the SFC session. Twenty minutes after the second SP test, we conducted a 5-min SFC session using the same ICR stimulus used for the Baseline test, but in a different spatial context. Importantly, only the ICR (CS^+), but not the C57BL/6J (CS^-) stimulus served for the SFC. Twenty minutes later, we conducted two SP tests with the same social stimuli as used before the SFC session (Early recall tests). The same tests with the same stimuli were then repeated 24 h later (Late recall tests). Examples of the subject's movement tracking during each of the paradigm stages are shown in Figure 4B. To examine whether social preference was significantly modified by the social fear conditioning, we conducted a 2 strains (C57BL/6J vs. ICR) x 2 stimuli (Empty vs. Social) 2-way mixed model (MM) ANOVA, for each of the stages. As for the Baseline stage, we found a significant main effect only for the stimulus, and a similarly significant preference was exhibited by the subjects toward both C57BL/6J and ICR stimuli, as compared to objects (Figure 4C). In contrast, during Early recall sessions, we found a significant interaction between stimulus and strain: while the subjects did not show any preference for C57BL/6J stimuli over objects, they developed a marginally significant avoidance toward the fear-conditioned ICR stimulus (Figure 4D). Moreover, at the Late recall stage, we found again a significant interaction between stimulus and strain, with *post hoc* analysis revealing a social preference for the C57BL/6J only (Figure 4E). Thus, while in the Baseline tests the subjects showed similar preference for both social stimuli, during the Late recall experiments, their behavior depended on the strain of the social stimulus.

When analyzing the theta rhythmicity recorded in the AHN during the Baseline and Late recall tests (using *Z* score analysis), we found a significant interaction between condition and strain (2-way MM ANOVA: Strain: $F_{(1,7)} = 4.691$; $p = 0.069$; Condition: $F_{(1,7)} = 0.264$, $p = 0.623$, Condition x Strain: $F_{(1,7)} = 6.223$, $p < 0.05$). While during Baseline, theta rhythmicity tended to be similarly elevated during sessions with both C57BL/6J and ICR stimuli (Figures 4F–4H), this was not the case during Late recall sessions. At this condition, we observed an augmented theta rhythmicity toward the C57BL/6J stimulus, as compared to Baseline, as opposed to a significantly reduced rhythmicity toward the fear-conditioned ICR stimulus (Figures 4J–4L). In contrast, no significant difference was observed between strains or stimuli for gamma rhythmicity (Figures S5B–S5G). Importantly, we observed no reduction in the average speed of the subject between the Baseline and Late recall tests and there was no difference in this variable between C57BL/6J and ICR stimuli during Late recall tests (Figures 4I and 4M), suggesting that the differences in theta rhythmicity could not be caused by differences in the subject's movement.

Thus, theta, but not gamma rhythmicity in the AHN seems to reflect the valence of the social stimulus during a social encounter, by showing enhancement during interaction with attractive stimuli, as compared to reduction in the presence of aversive stimuli.

Anterior hypothalamic nucleus c-Fos expression following social encounter does not differ between attractive and aversive stimuli

Unfortunately, we did not have enough MUA recorded during these experiments in order to reliably assess the spiking activity. Therefore, to examine the possibility that AHN neural activity during Late recall sessions differs between fear-conditioned and neutral social stimuli, we used c-Fos immunostaining as a proxy for neural activity. These experiments (n = 14 mice) were conducted with BALB/cJ mice serving as CS^+

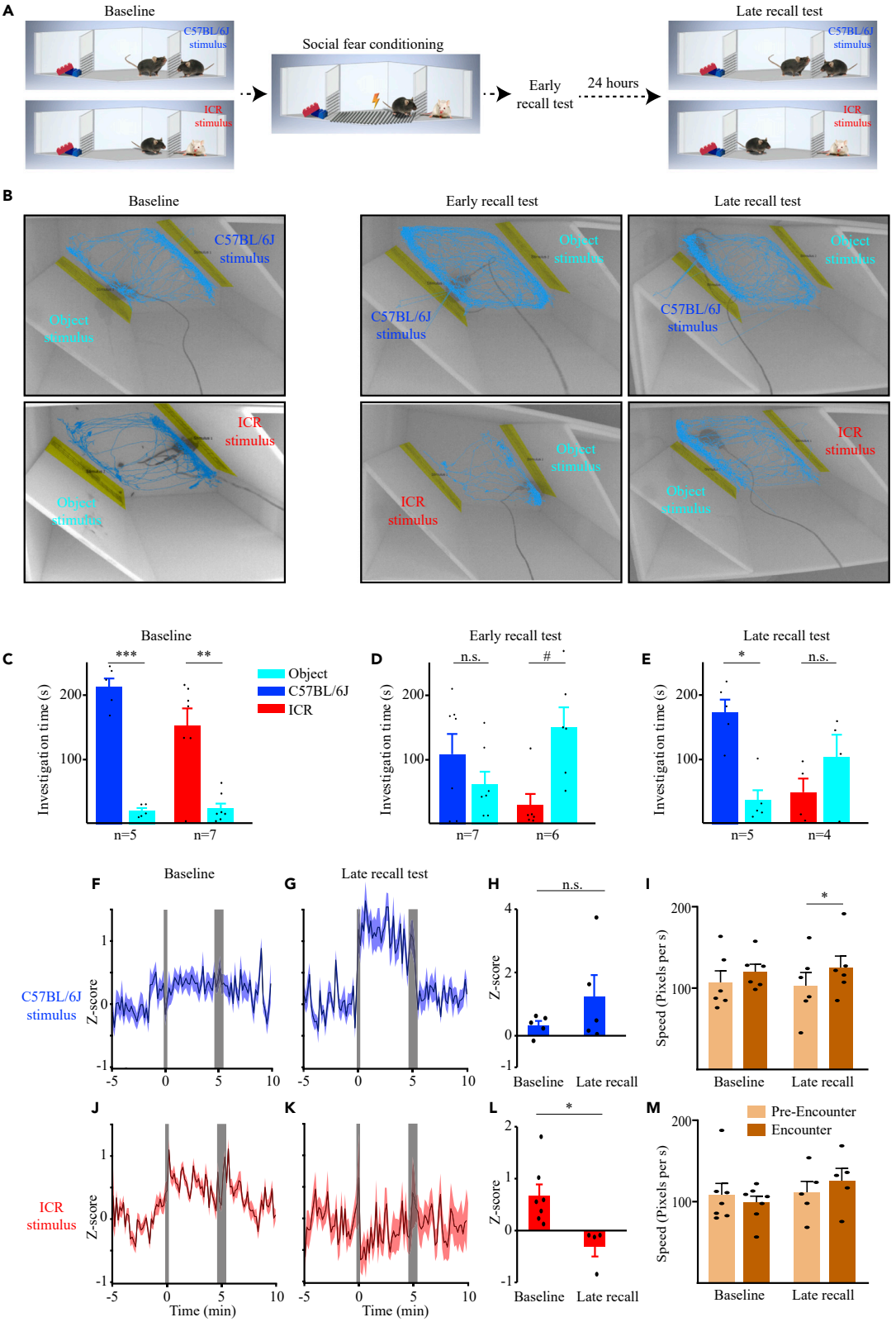
A
Baseline
C57BL/6J stimulus
ICR stimulus
Social fear conditioning
Early recall test
24 hours
Late recall test
B
Baseline
Early recall test
Late recall test
Object stimulus
C57BL/6J stimulus
ICR stimulus
C
Baseline
***
**
Object
C57BL/6J
ICR
Investigation time (s)
n=5
n=7
D
Early recall test
n.s.
#
n=7
n=6
E
Late recall test
*
n.s.
n=5
n=4
F
Baseline
G
Late recall test
C57BL/6J stimulus
Z-score
H
n.s.
Baseline
Late recall
I
*
Speed (Pixels per s)
J
ICR stimulus
K
Time (min)
L
*
M
Pre-Encounter
Encounter

Figure 4. Theta power of LFP signals in the AHN increases during affiliative social interactions and decreases during aversive ones

(A) A schematic depiction of the social fear conditioning (SFC) paradigm.

(B) Representative images of the arena and tracked movement of subject animals during the Baseline (left), Early recall (middle) and Late recall (right) conditions of the SFC paradigm, using either CS^- (C57BL/6J) or CS^+ (ICR) mice as social stimuli for the SP tests. The three stimuli are color coded (C57BL/6J – blue, ICR – red, object – light blue).

(C) Mean (±SEM) Investigation time dedicated to each of the stimuli during the Baseline SP tests. Note the similar results obtained with both C57BL/6J and ICR stimuli. Significant main effect in 2-way mixed model (MM) ANOVA was found for Stimulus ($p < 0.001$).

(D) As in C, for Early recall tests. Significant effect in 2-way MM ANOVA was found for Stimulus × Strain interaction ($p < 0.05$).

(E) As in C, for Late recall tests. Note the normal preference for the CS^- C57BL/6J mice, in contrast to the CS^+ ICR stimulus that draws no preference as compared to object stimuli. Significant main effect in 2-way MM ANOVA was found for Strain ($p < 0.05$) and Stimulus × Strain interaction ($p < 0.05$).

(F) Mean (±SEM) *Z* score analysis of theta power along the time course of the Baseline SP test using C57BL/6J mice.

(G) As in F, for the Late recall test using the same stimulus.

(H) Mean *Z* score (±SEM) analysis of the change in theta power during the Encounter stage of the SP test using C57BL/6J stimuli, calculated separately for Baseline (left) and Late recall (right) experiments. Note the apparent, but not statistically significant increase in theta power during Late recall, as compared to Baseline.

(I) Mean speed (±SEM) during the Pre-encounter and Encounter phases of the Baseline (left) and Late recall (right) SP tests using C57BL/6J stimuli, shown in F-G. Significant main effect in 3-way MM ANOVA was found for Time (Pre-encounter\Encounter) ($p < 0.05$).

(J) As in F, for ICR stimuli. (K) As in G, for ICR stimuli.

(L) As in H, for ICR stimuli. Note the statistically significant (Independent t-test: $p < 0.05$) reduction in theta power during the Late recall test, as compared to Baseline.

(M) As in I, for ICR stimuli. # = 0.07,*$p < 0.05$, **$p < 0.01$, ***$p < 0.001$ t-test with Bonferroni correction for multiple comparisons following a significant effect in ANOVA. See also Figure S6.

stimuli instead of ICR mice. This strain change did not alter the behavioral results (Figures 5A–5C), thus supporting the validity of the SFC paradigm across distinct strains of stimuli. When analyzing c-Fos expression in the AHN following a single Late recall test, we found a significantly higher number of c-Fos positive cells for both types of social stimuli, compared to control (no social stimulus during the Late recall test), with no significant difference between the CS^+ BALB/cJ and the CS^- C57BL/6J stimuli (Figures 5D and 5E). These results suggest that it is the theta rhythmicity in the AHN, rather than the level of spiking activity, which reflects the valence of the social stimulus during social encounters.

Optogenetic stimulation of anterior hypothalamic nucleus neurons in a social context modulates approach behavior

To directly assess the role of the AHN in social approach or avoidance behaviors, we used the optogenetic stimulation of AHN neurons in mice that were injected with a ChR2.0-expressing AAV viral vector and chronically implanted with optic fibers into the AHN (Figures 6A and 6B). In slice whole-cell patch recordings, infected AHN neurons responded to 1-ms optogenetic stimulation at various rates with spiking activity that followed the stimulation frequency quite well between 5 and 20 Hz stimulation, but not so well above 20 Hz (Figures 6C and 6D). Interestingly, AHN neurons were characterized by a prominent afterdepolarization component, which in many cases generated the firing of spike doublets (Figure 6C).

Four weeks after the viral infection and implantation of an optic fiber, mouse subjects (n = 9 mice) were subjected to SP tests in which the animals were either unstimulated (Figure 6E), stimulated at the beginning of social investigation bouts (Figure 6F), or stimulated when being near the object stimulus (Figure 6G). Each stimulation was given as a 20 Hz train of 20 ms light pulses, lasting for 1 s. The three types of experiments were randomly conducted with the same animals, each on a separate day. Optogenetic stimulation was given on average 13 times in a session for each type of stimulation condition, with no significant difference between them (Independent samples t-test, $t_{13} = -0.308$, $p = 0.763$). When analyzing the investigation time dedicated to each of the stimuli across the various stimulation conditions (during the first 2 min of the session), we found a significant interaction between stimulus and condition. As expected, unstimulated animals exhibited a clear social preference throughout the test (Figures 6E and 6H). Similar results were observed with animals that were stimulated during the social investigation (Figures 6F and 6H). In contrast, animals that were stimulated while being near the object stimulus showed no social preference (Figures 6G and 6H). Similar results were obtained when we analyzed data obtained only from animals that passed through all stimulation conditions (Figures S6A–S6D, n = 6 mice). Notably, no difference in total investigation time (Social + object) was observed between the various stimulation protocols, suggesting no general effect on stimulus investigation behavior (Between-Subjects ANOVA: $F_{(2,21)} = 1.447$, $p = 0.258$). Moreover, stimulating near the object caused a significantly higher time of object investigation as compared to stimulation during social investigation, while the opposite effect was observed for social investigation time

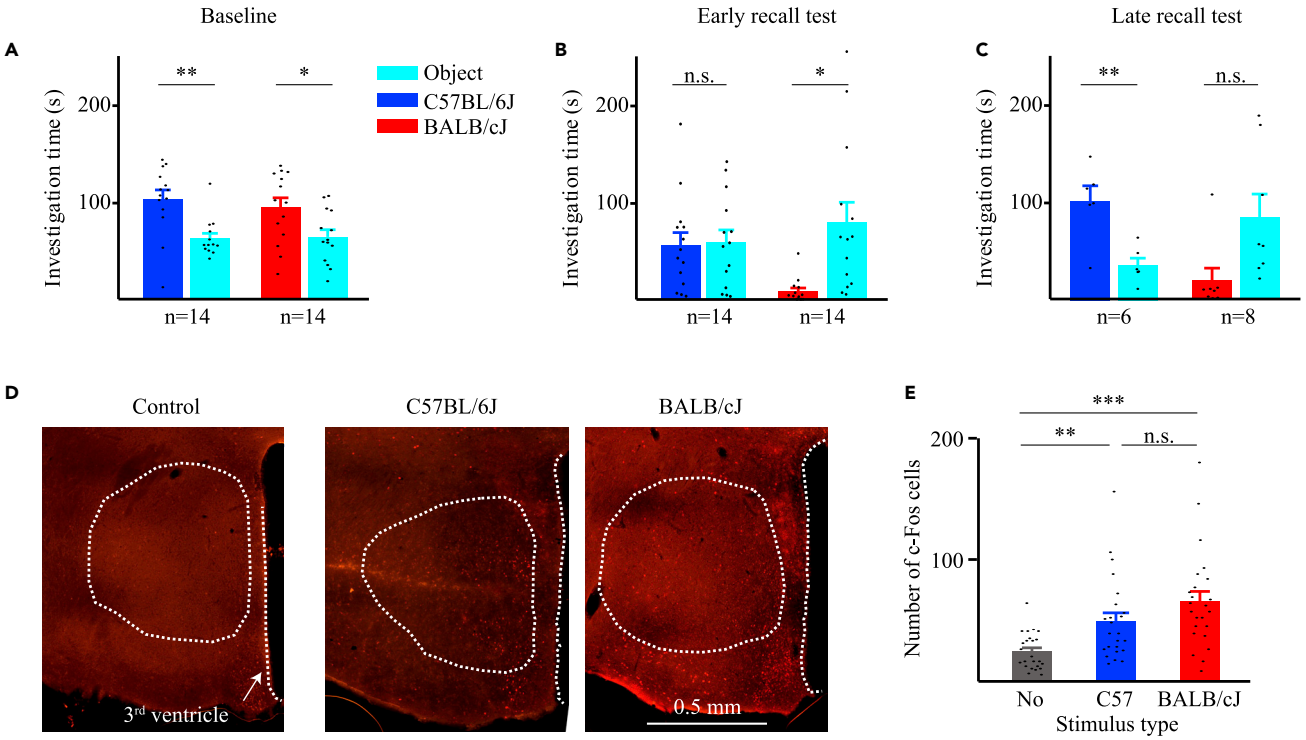

Figure 5. No difference in AHN c-Fos expression following affiliative vs. aversive social interaction

(A) Mean (±SEM) investigation time during Baseline SP tests conducted with either C57BL/6J or BALB/cJ social stimuli before SFC. Significant main effect in 2-way MM ANOVA was found for Stimulus ($p < 0.001$).

(B) As in A, for Early recall tests. Significant main effect in 2-way MM ANOVA was found for Stimulus ($p < 0.05$), and Stimulus × Strain interaction ($p < 0.05$).

(C) As in A, for Late recall tests. Significant effect in 2-way MM ANOVA was found for Stimulus× Strain interaction ($p < 0.01$).

(D) Representative images depicting c-Fos immunostaining in the AHN of animals after a Late recall test conducted using either no social stimulus (control, left), C57BL/6J social stimulus (middle), or BALB/cJ social stimulus (right). Note the similar number of stained cells in the latter two cases.

(E) Mean (±SEM) number of c-Fos expressing cells after Late recall tests using either no social stimulus (control, gray), C57BL/6J social stimulus (middle, blue), or BALB/cJ social stimulus (right, red). Note that both social stimuli elicited a similar significant increase in c-Fos-positive cell number, as compared to the control. Significant main effect was found in Kruskal-Wallis test ($p < 0.001$). *$p < 0.05$,**$p < 0.01$, ***$p < 0.001$, paired t-test with Bonferroni correction for multiple comparisons following main effect in ANOVA, or Dunn's multiple comparisons following the main effect in Kruskal-Wallis test for non-parametric comparisons.

(*Social Investigation time*- Between-Subjects ANOVA: $F_{(2,21)} = 4.191$, $p < 0.05$; *post hoc* Bonferroni comparisons: No stim. Vs. Stim. with social: $p = 0.714$; No stim. Vs. Stim. near object: $p = 0.263$; Stim. with social Vs. Stim. near object: $p < 0.05$; *Object Investigation time*- Between-Subjects ANOVA: $F_{(2,21)} = 3.988$, $p < 0.05$; *post hoc* Bonferroni comparisons: No stim. Vs. Stim. with social: $p = 0.3$; No stim. Vs. Stim. near object: $p = 0.714$; Stim. with social Vs. Stim. near object: $p < 0.05$). Thus, it seems as if stimulating near a given stimulus enhances its investigation by the stimulated subject.

To further analyze these data, we plotted the cumulative investigation time as a function of investigation bout duration in all three conditions, separately for each stimulus. As apparent, there was a significant difference between the three conditions for both stimuli (Figures 6I and 6J). Interestingly, optogenetic stimulation of AHN neurons near the social stimulus shifted the social investigation toward a higher number of short bouts, compared to both other conditions (Figures 6I and 6J). We, therefore, summed the investigation time dedicated to each stimulus separately for short (≤6 s) and long (>6 s) bouts, as we have previously described.[26] In accordance with our previous results, unstimulated animals did not show any difference between stimuli in short bouts, and their social preference was reflected only in investigation bouts which were longer than 6 s (Figure 6K). In contrast, the social preference of animals stimulated near the social stimulus was reflected by both short and long bouts (Figure 6L). Animals stimulated near the object did not show any social preference (Figure 6M).

To further explore the possibility that AHN stimulation near the social stimulus shifted the social investigation toward a higher number of bouts, we compared the number of investigation bouts between the

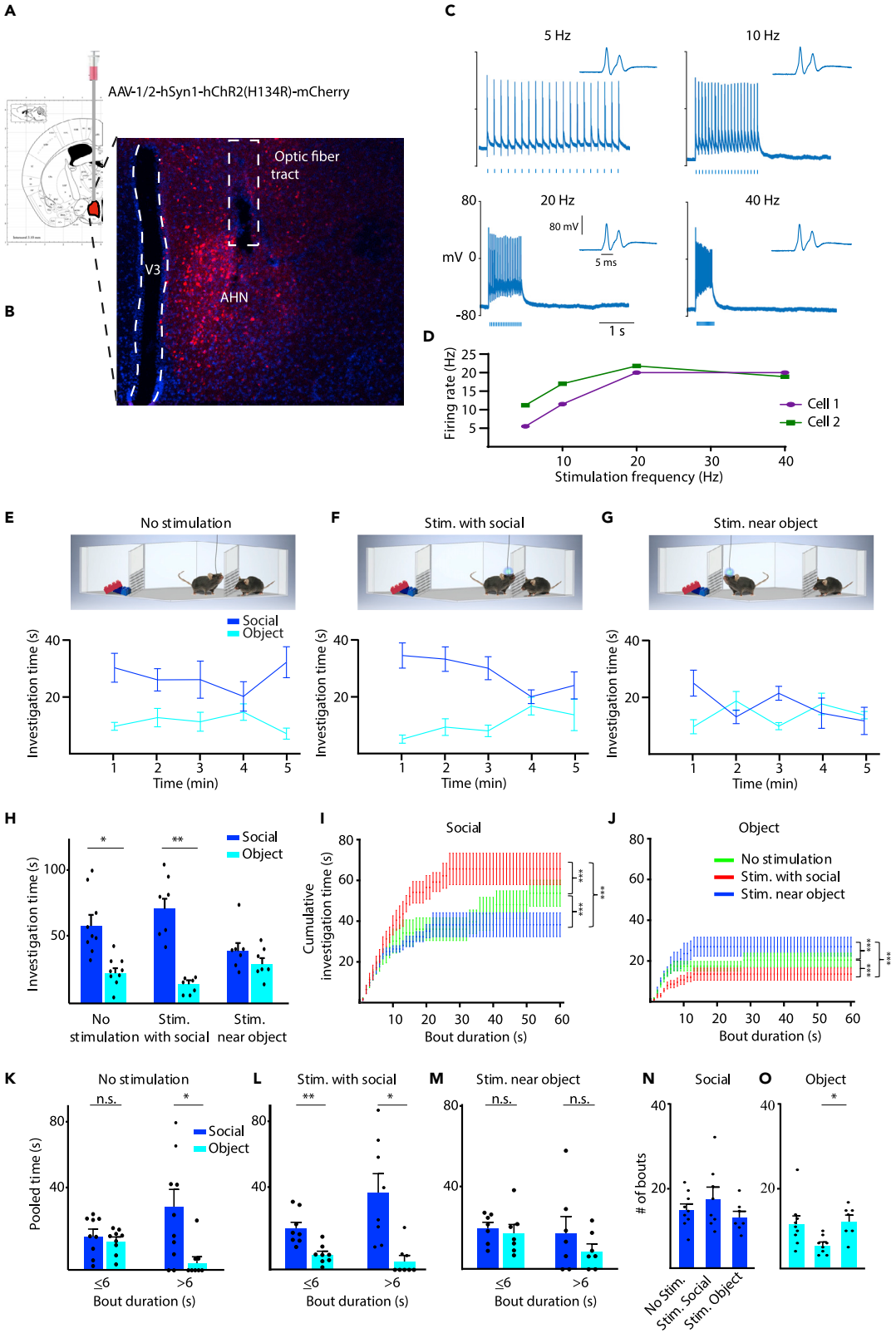
A
AAV-1/2-hSyn1-hChR2(H134R)-mCherry
Optic fiber tract
V3
AHN
B
C
5 Hz
10 Hz
20 Hz
40 Hz
80 mV
5 ms
mV 0
80
-80
1 s
D
Firing rate (Hz)
Cell 1
Cell 2
Stimulation frequency (Hz)
E
No stimulation
F
Stim. with social
G
Stim. near object
Social
Object
Investigation time (s)
Time (min)
H
Investigation time (s)
No stimulation
Stim. with social
Stim. near object
I
Social
Cumulative investigation time (s)
Bout duration (s)
J
Object
No stimulation
Stim. with social
Stim. near object
K
No stimulation
Pooled time (s)
n.s.
Bout duration (s)
L
Stim. with social
M
Stim. near object
N
Social
# of bouts
O
Object
No Stim.
Stim. Social
Stim. Object

Figure 6. Optogenetic stimulation of AHN neurons during the SP test modulates the investigation of the stimulus associated with the activation

(A) A scheme of the viral injection to the AHN.

(B) Representative image of AHN in a brain slice, depicting the infected neurons and optic fiber location.

(C) Electrophysiological traces exemplifying whole-cell patch recording from a viral-infected AHN neuron in response to optogenetic stimulation at various rates (noted above the traces). The inset on the right of each trace shows the response to the first stimulus in higher time resolution, exposing a spike doublet.

(D) The mean firing rate across the stimulation epoch, as a function of the stimulation frequency. Note the almost linear relationship observed between frequencies of 5-20 Hz.

(E) Mean (±SEM) investigation time across the SP session (1-min bin) for each stimulus, plotted for the no optogenetic stimulation (control) condition (schematically depicted above). Note the clear social preference exhibited by the subjects.

(F) As in E, for optogenetic stimulation given during social investigation bouts.

(G) As in E, when stimulation was given near the object (away from the social stimulus). Note the loss of social preference specifically in this condition.

(H) Mean (±SEM) investigation time throughout the session for the three conditions shown in E-G. Significant main effect in 2-way MM ANOVA was found for Stimulus ($p < 0.001$) and Stimulus × Condition interaction ($p < 0.05$).

(I) Cumulative histogram (mean ± SEM) of social investigation time plotted as a function of investigation bout duration, separately for the three stimulation conditions (color-coded). Note the statistically significant differences between the three curves (***$p < 0.001$, Kolmogorov-Smirnov test).

(J) As in I, for object investigation bouts. Note the inverse relationship between the curves as compared to I.

(K) Mean (±SEM) investigation time was pooled separately for short (≤6 s) and long (>6 s) investigation bouts, for each of the investigated stimuli during the control condition. Significant main effect in 2-way RM ANOVA was found for Stimulus ($p < 0.01$) and Stimulus × Bout duration interaction ($p < 0.05$). Note the insignificant difference between social and object stimuli for short bouts.

(L) As in K, for stimulation during social investigation. Note the significant difference between social and object stimuli even for short bouts. Significant main effect in 2-way RM ANOVA was found for Stimulus ($p < 0.001$). Note the insignificant difference between social and object stimuli for short bouts.

(M) As in K, for stimulation near the object. Note that none of the bout durations showed any significant difference between the social and object stimuli.

(N) Mean (±SEM) number of social investigation bouts for each one on the stimulation conditions.

(O) As in N, for object investigation bouts. Significant main effect in 1-way ANOVA was found for Condition (*$p < 0.05$). Note the significant increase observed for stimulation near the object, as compared to stimulation near the social stimulus. *$p < 0.05$, **$p < 0.01$, ***$p < 0.001$, paired t-test with Bonferroni correction for multiple comparisons following the main effect in ANOVA. See also Figure S6.

stimulation conditions, separately for each stimulus. While we found no significant change for the social stimulus (Figure 6N), the number of bouts toward the object was significantly higher when the subjects were stimulated near the object, as compared to when they were stimulated during social investigation (Figure 6O).

In order to make sure that the effect of AHN optogenetic stimulation during the SP test is not confounded by the movement of the social stimulus, as opposed to the inanimate object, we conducted similar experiments using the sex-preference (SxP) task (n = 5 mice). In this task, the subject mouse is tested for its preference between a male and a female conspecific, thus between two social stimuli. Normally, C57BL/6J adult male subjects prefer a female over a male stimulus.[28,29] Here we conducted this task while optogenetically stimulating AHN neurons when the subject started investigating either the male or the female (Figures 7A and 7B). While a clear preference toward investigating the female was exhibited by the male subjects when stimulated during the investigation of the preferred stimulus (female), no preference was observed when the animals were stimulated while investigating the less-preferred stimulus (male) (Figure 7C). In a similar manner to the SP test, the difference between the two stimulation protocols was mainly at the first 2-3 min of the task (Figures 7A and 7B). Moreover, the two protocols yielded significantly distinct distributions of investigation bouts during the first 2 min of the task (Figures 7D and 7E), with stimulation near the male causing less time in long investigation bouts toward the female and more time in short investigation bots toward the mail (Figure 7F). As in the case of the SP test (Figures 6N and 6O), we found in the SxP test no change in the number of bouts toward the preferred stimulus (female), but observed a significant increase in the number of bouts toward the less-preferred stimulus (male), for stimulation near the male, as compared to stimulation near the female. Thus, optogenetic stimulation of AHN neurons changed the subject's investigation pattern in favor of the stimulus associated with the stimulation, especially if this stimulus was the less-preferred one. Altogether, these results support a role for AHN neural activity in regulating approach behavior in a social context.

DISCUSSION

Here we combined *in vivo* electrophysiology in behaving mice with c-Fos staining and optogenetic stimulation to probe the function of AHN neurons in social behavior. Specifically, we examined their role in regulating approach and avoidance behaviors during various social tasks. Overall, our results suggest that in affiliative social contexts, synchronized activity of AHN neurons is associated with approach behavior.

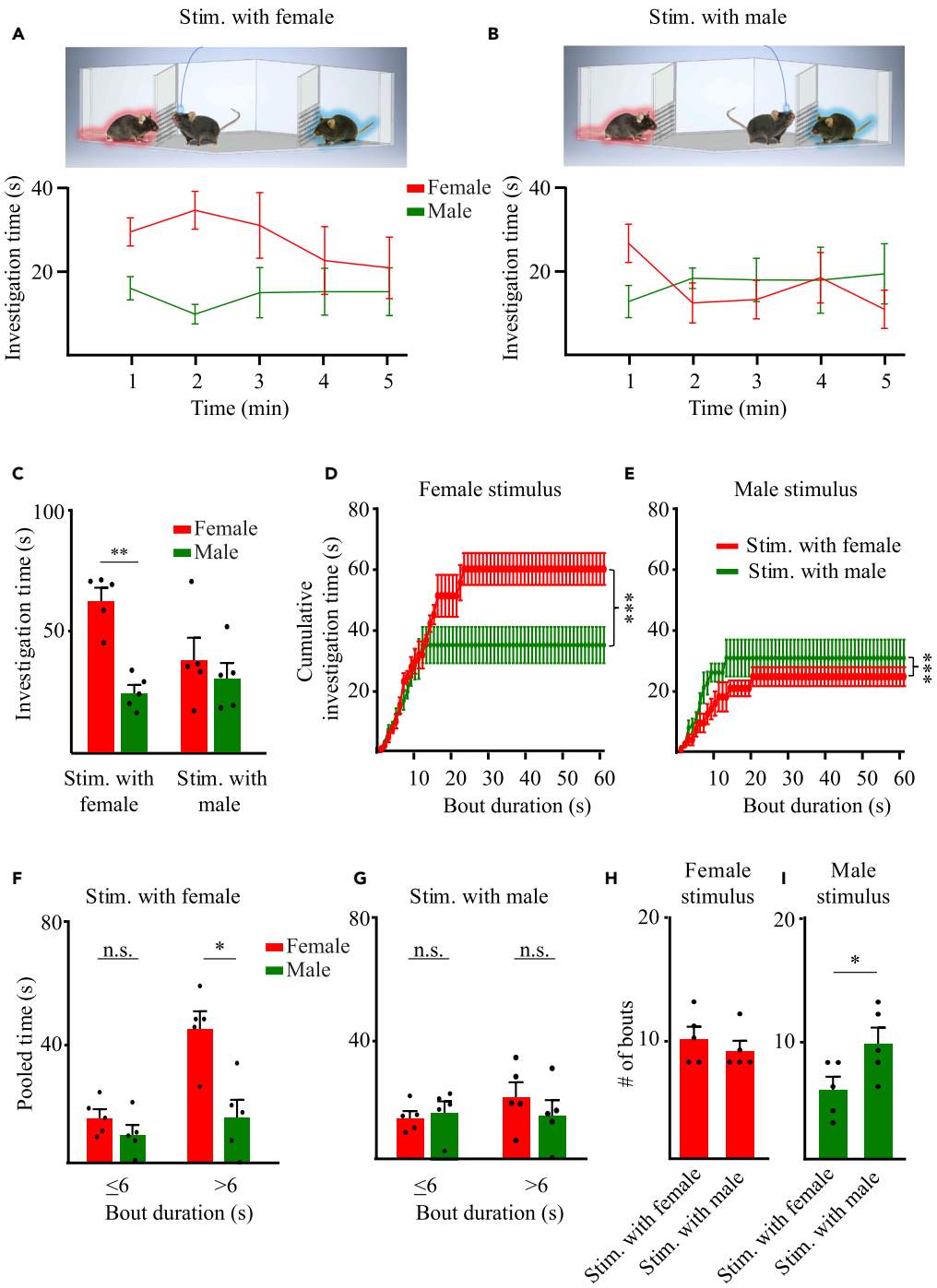

Figure 7. AHN Optogenetic stimulation during the sex-preference (SxP) test also modulates the investigation of the stimulus associated with the stimulation

(A) Mean (±SEM) investigation time across the SP session (1-min bin) for each stimulus, plotted for optogenetic stimulation near the female condition (schematically depicted above). Note the clear sex preference exhibited by the subjects.

(B) As in A, for optogenetic stimulation near the male. Note the lack of any sex preference in this condition.

(C) Mean (±SEM) investigation time throughout the session for the two conditions shown in A-B. Significant main effect in 2-way MM ANOVA was found for Condition ($p < 0.05$). **$p < 0.01$, paired t-test with Bonferroni correction following the main effect in ANOVA.

Figure 7. *Continued*

(D) Cumulative histogram (mean ± SEM) of female investigation time plotted as a function of investigation bout duration, separately for the three two conditions (color-coded). Note the statistically significant difference between the two curves (***$p < 0.001$, Kolmogorov-Smirnov test).

(E) As in I, for male investigation. Note the inverse relationship between the curves as compared to I.

(F) Mean (±SEM) investigation time pooled separately for short (≤6 s) and long (>6 s) investigation bouts, for each of the investigated stimuli during the control condition. Significant main effects in 2-way RM ANOVA were found for Stimulus ($p < 0.01$), and Bout duration × Stimulus interaction ($p < 0.05$). *$p < 0.05$, paired t-test with Bonferroni correction following the main effect in ANOVA.

(G) As in K, for stimulation during the social investigation. Note the insignificant difference between female and male stimuli for both bout durations.

(H) Mean (±SEM) number of female investigation bouts for each one on the stimulation conditions.

(I) As in N, for male investigation bouts. Note the significant increase observed for stimulation near the male, as compared to stimulation near the female. Independent t-test (*$p < 0.05$).

In accordance with our previous study in rats,[30] our current results show that the social context is reflected mainly by LFP theta rhythmicity, which was elevated during affiliative interaction and reduced during aversive interaction. The differences in theta rhythmicity between affiliative and aversive interactions were not accompanied by differences in the movement of the subject, hence seem to reflect the affective state of the animal rather than its motor activity. It should be noted that elevation in AHN theta rhythmicity is not necessarily restricted to social interactions, and may be functional in non-social contexts just as well. Nevertheless, LFP theta and gamma power in the AHN did not change markedly during investigation bouts toward the various stimuli. Thus, LFP rhythmicity in the AHN does not seem to be associated with specific behavioral events, but rather with the social context. These results differ from the results of similar recordings we have performed in the murine medial amygdala (MeA), where we found that theta and gamma rhythmicity significantly increases during social investigation bouts.[31] Therefore, our data suggest distinct roles for rhythmic LFP in the MeA and AHN of adult male mice during social interactions, with AHN rhythmic activity reflecting the social context while MeA rhythmicity reflecting social investigation. This difference may be dictated by the strong and direct input arriving at the MeA from the accessory olfactory bulb, the first brain region that processes pheromonal information detected by the vomeronasal organ during social investigation.[32]

In contrast to the general increase in LFP theta and gamma rhythmicity, we found spiking activity in the AHN to be generally reduced in a social context. Such an overall reduction in spiking activity may support enhanced signal-to-noise ratio (SNR) of AHN neuronal responses during investigation bouts. Such a phenomenon, which may be dictated by the synchronizing effect of LFP rhythmicity,[33] is well-known in other brain areas.[34,35] Nevertheless, we found that spiking activity in the AHN is specifically modified during investigation behavior, in a stimulus-dependent manner. While the spiking response rapidly declined during object investigation, during social investigation it was kept above baseline for several seconds. This significant stimulus effect was not due to the fact that investigation bouts toward social stimuli tend to be longer than toward objects,[26] as we observed the same effect when we separately analyzed long investigation bouts. Since the subject mice preferred investigating the social stimulus as compared to the object, the higher spiking activity of AHN neurons during social investigation strongly suggests that in a social context, AHN neural activity is associated with approach behavior rather than avoidance. These results are consistent with the results of both Anthony et al.[24] and of Xie et al.[18] Moreover, they do not contradict the multiple studies conducted with various rodent species, which implicated the AHN in aggressive behavior,[23,36–38] as such behavior also requires approach toward social stimuli. Thus, AHN neural activity may modulate approach behavior toward stimuli in the affiliative social context, regardless of whether in affiliative or aggressive manner. Future studies may tell whether this effect is due to a general decrease in anxiety, a specific reduction in fear from approach, or an increased negative value of avoidance.

Employing stimulus-specific SFC that enables modifying the valence of a specific social stimulus from attractive to aversive, we compared the responses of AHN neurons between attractive and aversive social stimuli. Our c-Fos analysis indicates a similar number of AHN neurons activated during encounters with both types of social stimuli. It is possible that distinct neuronal ensembles are activated by the opposite types of social stimuli, one of which is associated with approach behavior while the other triggers avoidance. It should be noted that such an arrangement was recently demonstrated in the PAG,[39] one of the main targets of the AHN.[40,41] Alternatively, the same neurons may be activated by both stimuli, but in a different manner. Notably, we found that in social contexts, AHN spiking activity exhibited enhanced theta

rhythmicity and was synchronized with the LFP theta rhythmicity. Thus, both attractive and aversive social stimuli may trigger similar firing rates of AHN neurons, hence a similar level of c-Fos expression. Yet, in the affiliative social context, the enhanced LFP theta rhythmicity may impose more coherent spiking activity in the AHN, which would drive the animals toward the social approach. In contrast, non-coherent AHN activity driven by aversive stimuli may fail to induce approach behavior or even elicit avoidance.

In accordance with this suggestion, the coherent activation of AHN neurons by our optogenetic stimulation drove the subject animal to interact with the stimulus associated with optogenetic activation. This was especially prominent for stimuli that were naturally less preferred, such as the object in the SP test or the male in the SxP test. Interestingly, we found that optogenetic stimulation near these stimuli induced an elevation in the number of investigation bouts toward them. These results are in accordance with the role of AHN neuronal activity in initiating approach behavior toward nearby stimuli. The reason why we did not observe such a stimulation-induced elevation in the number of investigation bouts toward the preferred stimuli too, may be due to a ceiling effect in the investigation of these stimuli. It should be noted that, following the stimulation protocol of a previous study,[24] we applied optogenetic stimulation at 20 Hz pulses, which is beyond the range of theta rhythmicity (4-12 Hz). Thus, it might be that while inducing coherent neural activity, our stimulation protocol also interfered with the intrinsic theta rhythmicity of the AHN and abolished it. Therefore, we cannot draw a causal link between AHN theta rhythmicity and approach behavior.

In previous studies, direct optogenetic stimulation of AHN neurons caused distinct responses, in a context-dependent manner. These included escape in an empty arena, biting attack following a mechanical stimulation, and enhanced social investigation in a social context.[16,18] In light of all these studies, our results are consistent with the idea that the behavioral effect of AHN activation is highly context-dependent. How exactly the type of context affects the consequences of AHN activity should be explored in future studies. Yet, we suggest that one mechanism which may be involved in regulating context-dependent neural activity is the frequency and level of theta rhythmicity and the synchronized activity it may impose on various brain regions. It should be noted that in our previous study where we used multi-site brain recording from behaving rats, we found that social and fear stimuli induce theta rhythmicity in different frequencies and distinct patterns of theta coherence in some regions of the SBN.[30] Such brain-region specific modulation of theta rhythmicity and its coherence may therefore encode various emotional contexts and guide distinct outcomes of activity in the relevant brain regions.

Limitations

We note a number of methodological limitations in our study. First, the optogenetic stimulation protocol used for the excitation of AHN during SP and SxP consisted of 20Hz pulses, which is beyond the range of theta rhythmicity (4-12 Hz). Hence, it might be that while inducing coherent neural activity, our stimulation protocol also interfered with the intrinsic theta rhythmicity of the AHN and abolished it. Therefore, we cannot draw a causal link between AHN theta rhythmicity and approach behavior. Second, the sample size in our SFC with electrophysiology recordings was too modest (n = 5) to enable enough MUA sampling for the reliable assessment of the spiking activity across the various conditions of the paradigm. This problem did not allow us to reveal how the correlation between spiking activity and theta rhythmicity, like the one observed in SP, might have changed in social interactions with stimuli of different valence. Third, in this study, which employed *in vivo* electrophysiology and optogenetics in the hypothalamus of behaving mice, we could explore only a low number of animals. To avoid possible confounding effects of the ovulation cycle in females, which is most prominent in the hypothalamus, we have limited our recordings to males only. Thus, future studies may reveal sex-dependent changes in the activity of AHN neurons during social behavior. Lastly, it should be noted that while our study centers on changes in neural activity dynamics of the AHN in social contexts, our data do not provide information regarding the molecular profile of the cells driving the recorded activity measured in our experiments. Therefore, future studies using cell-type specific neural activity recording can help identify possible interplays between different subpopulations of the AHN that drive its activity in various contexts.

Summary

Here we found that in an affiliative social context, AHN neural activity is getting more rhythmic and is enhanced during the investigation of social, but not object stimuli. We also showed that AHN theta rhythmicity is elevated during affiliative, but not aversive social interactions. Finally, we demonstrated that the direct optogenetic stimulation of AHN neurons modulated approach behavior toward stimuli associated

with this stimulation, especially for less-preferred stimuli. Overall, our results suggest a role for AHN neural activity in regulating approach behavior during social interactions, and for theta rhythmicity in mediating the valence of the social context.

STAR★METHODS

Detailed methods are provided in the online version of this paper and include the following:

- KEY RESOURCES TABLE
- RESOURCE AVAILABILITY
  - Lead contact
  - Materials availability
  - Data and code availability
- EXPERIMENTAL MODEL AND SUBJECT DETAILS
  - Animals
  - Institutional review board
- METHOD DETAILS
  - Experiments
  - Experimental setups
  - Behavioral paradigms
  - Electrode implantation surgery
  - Electrophysiological recordings
  - *In vivo* optogenetic stimulation
  - *In vitro* electrophysiology
  - c-Fos expression
  - Microscopy
- QUANTIFICATION AND STATISTICAL ANALYSIS
  - Tracking software and behavioral analyses
  - Analysis of LFP signals
  - Analysis of spiking activity
  - Spike-triggered LFP (stLFP) analysis
  - Statistical analysis

SUPPLEMENTAL INFORMATION

Supplemental information can be found online at https://doi.org/10.1016/j.isci.2022.105921.

ACKNOWLEDGMENTS

We thank Boris Shklyar, Head of Bioimaging Unit, and Alex Bizer, the experimental systems engineer of the Faculty of Natural Sciences of the University of Haifa, for their help. We also thank Dr. Yair Shemesh from the Weizmann Institute, Rehovot, Israel, for the critical reading of the manuscript draft. This study was supported by the ISF-NSFC joint research program (grant No. 3459/20 to SW), the Israel Science Foundation (grant No. 1361/17 to SW), the Ministry of Science, Technology and Space of Israel (Grant No. 3-12068 to SW) and the United States-Israel Binational Science Foundation (grant No. 2019186 to SW).

AUTHOR CONTRIBUTIONS

Conceptualization (SN, SW), methodology (SN), software (SN), validation (SN, SW), formal analysis (RJ, SN, SS, WD), investigation (BKP, RJ, SN, SS, WD), resources (EB), writing – original draft (RJ, SN, SW), writing – review & editing (EB, SN, SW), visualization (RJ, SN), supervision (SW), project administration (SN), and funding acquisition (SW).

DECLARATION OF INTERESTS

The authors declare no competing interests.

INCLUSION AND DIVERSITY

We support inclusive, diverse, and equitable conduct of research.

Received: July 19, 2022
Revised: November 17, 2022
Accepted: December 29, 2022
Published: February 17, 2023

REFERENCES

1. Adolphs, R. (2010). Conceptual challenges and directions for social neuroscience. Neuron *65*, 752–767. https://doi.org/10.1016/j.neuron.2010.03.006.

2. Carnevali, L., Montano, N., Tobaldini, E., Thayer, J.F., and Sgoifo, A. (2020). The contagion of social defeat stress: insights from rodent studies. Neurosci. Biobehav. Rev. *111*, 12–18. https://doi.org/10.1016/j.neubiorev.2020.01.011.

3. Ferretti, V., and Papaleo, F. (2019). Understanding others: emotion recognition in humans and other animals. Gene Brain Behav. *18*, e12544. https://doi.org/10.1111/gbb.12544.

4. Ford, C.L., and Young, L.J. (2021). Translational opportunities for circuit-based social neuroscience: advancing 21st century psychiatry. Curr. Opin. Neurobiol. *68*, 1–8. https://doi.org/10.1016/j.conb.2020.11.007.

5. Kohl, J., and Dulac, C. (2018). Neural control of parental behaviors. Curr. Opin. Neurobiol. *49*, 116–122. https://doi.org/10.1016/j.conb.2018.02.002.

6. Lee, C.R., Chen, A., and Tye, K.M. (2021). The neural circuitry of social homeostasis: consequences of acute versus chronic social isolation. Cell *184*, 2794–2795. https://doi.org/10.1016/j.cell.2021.04.044.

7. McKinsey, G., Ahmed, O.M., and Shah, N.M. (2018). Neural control of sexually dimorphic social behaviors. Curr. Opin. Physiol. *6*, 89–95. https://doi.org/10.1016/j.cophys.2018.08.003.

8. Olsson, A., Knapska, E., and Lindström, B. (2020). The neural and computational systems of social learning. Nat. Rev. Neurosci. *21*, 197–212. https://doi.org/10.1038/s41583-020-0276-4.

9. Wei, D., Talwar, V., and Lin, D. (2021). Neural circuits of social behaviors: innate yet flexible. Neuron *109*, 1600–1620. https://doi.org/10.1016/j.neuron.2021.02.012.

10. Dickinson, S.Y., Kelly, D.A., Padilla, S.L., and Bergan, J.F. (2022). From reductionism toward integration: understanding how social behavior emerges from integrated circuits. Front. Integr. Neurosci. *16*, 862437. https://doi.org/10.3389/fnint.2022.862437.

11. Goodson, J.L. (2005). The vertebrate social behavior network: evolutionary themes and variations. Horm. Behav. *48*, 11–22. https://doi.org/10.1016/j.yhbeh.2005.02.003.

12. Anderson, D.J. (2012). Optogenetics, sex, and violence in the brain: implications for psychiatry. Biol. Psychiatr. *71*, 1081–1089. https://doi.org/10.1016/j.biopsych.2011.11.012.

13. Hashikawa, K., Hashikawa, Y., Falkner, A., and Lin, D. (2016). The neural circuits of mating and fighting in male mice. Curr. Opin. Neurobiol. *38*, 27–37. https://doi.org/10.1016/j.conb.2016.01.006.

14. Matthews, G.A., and Tye, K.M. (2019). Neural mechanisms of social homeostasis. Ann. N. Y. Acad. Sci. *1457*, 5–25. https://doi.org/10.1111/nyas.14016.

15. Canteras, N.S. (2002). The medial hypothalamic defensive system: hodological organization and functional implications. Pharmacol. Biochem. Behav. *71*, 481–491. https://doi.org/10.1016/s0091-3057(01)00685-2.

16. Bang, J.Y., Sunstrum, J.K., Garand, D., Parfitt, G.M., Woodin, M., Inoue, W., and Kim, J. (2022). Hippocampal-hypothalamic circuit controls context-dependent innate defensive responses. Elife *11*, e74736. https://doi.org/10.7554/eLife.74736.

17. Wang, L., Chen, I.Z., and Lin, D. (2015). Collateral pathways from the ventromedial hypothalamus mediate defensive behaviors. Neuron *85*, 1344–1358. https://doi.org/10.1016/j.neuron.2014.12.025.

18. Xie, Z., Gu, H., Huang, M., Cheng, X., Shang, C., Tao, T., Li, D., Xie, Y., Zhao, J., Lu, W., et al. (2022). Mechanically evoked defensive attack is controlled by GABAergic neurons in the anterior hypothalamic nucleus. Nat. Neurosci. *25*, 72–85. https://doi.org/10.1038/s41593-021-00985-4.

19. Risold, P.Y., Canteras, N.S., and Swanson, L.W. (1994). Organization of projections from the anterior hypothalamic nucleus: a Phaseolus vulgaris-leucoagglutinin study in the rat. J. Comp. Neurol. *348*, 1–40. https://doi.org/10.1002/cne.903480102.

20. Cezario, A.F., Ribeiro-Barbosa, E.R., Baldo, M.V.C., and Canteras, N.S. (2008). Hypothalamic sites responding to predator threats–the role of the dorsal premammillary nucleus in unconditioned and conditioned antipredatory defensive behavior. Eur. J. Neurosci. *28*, 1003–1015. https://doi.org/10.1111/j.1460-9568.2008.06392.x.

21. Martinez, R.C.R., Carvalho-Netto, E.F., Amaral, V.C.S., Nunes-de-Souza, R.L., and Canteras, N.S. (2008). Investigation of the hypothalamic defensive system in the mouse. Behav. Brain Res. *192*, 185–190. https://doi.org/10.1016/j.bbr.2008.03.042.

22. Mendes-Gomes, J., Motta, S.C., Passoni Bindi, R., de Oliveira, A.R., Ullah, F., Baldo, M.V.C., Coimbra, N.C., Canteras, N.S., and Blanchard, D.C. (2020). Defensive behaviors and brain regional activation changes in rats confronting a snake. Behav. Brain Res. *381*, 112469. https://doi.org/10.1016/j.bbr.2020.112469.

23. Tachikawa, K.S., Yoshihara, Y., and Kuroda, K.O. (2013). Behavioral transition from attack to parenting in male mice: a crucial role of the vomeronasal system. J. Neurosci. *33*, 5120–5126. https://doi.org/10.1523/JNEUROSCI.2364-12.2013.

24. Anthony, T.E., Dee, N., Bernard, A., Lerchner, W., Heintz, N., and Anderson, D.J. (2014). Control of stress-induced persistent anxiety by an extra-amygdala septohypothalamic circuit. Cell *156*, 522–536. https://doi.org/10.1016/j.cell.2013.12.040.

25. Netser, S., Haskal, S., Magalnik, H., Bizer, A., and Wagner, S. (2019). A system for tracking the dynamics of social preference behavior in small rodents. J. Vis. Exp. https://doi.org/10.3791/60336.

26. Netser, S., Haskal, S., Magalnik, H., and Wagner, S. (2017). A novel system for tracking social preference dynamics in mice reveals sex- and strain-specific characteristics. Mol. Autism. *8*, 53. https://doi.org/10.1186/s13229-017-0169-1.

27. Fries, P. (2015). Rhythms for cognition: communication through coherence. Neuron *88*, 220–235. https://doi.org/10.1016/j.neuron.2015.09.034.

28. de la Zerda, S.H., Netser, S., Magalnik, H., Briller, M., Marzan, D., Glatt, S., Abergel, Y., and Wagner, S. (2022). Social recognition in laboratory mice requires integration of behaviorally-induced somatosensory, auditory and olfactory cues. Psychoneuroendocrinology *143*, 105859. https://doi.org/10.1016/j.psyneuen.2022.105859.

29. Kopachev, N., Netser, S., and Wagner, S. (2022). Sex-dependent features of social behavior differ between distinct laboratory mouse strains and their mixed offspring. iScience *25*, 103735. https://doi.org/10.1016/j.isci.2022.103735.

30. Tendler, A., and Wagner, S. (2015). Different types of theta rhythmicity are induced by social and fearful stimuli in a network associated with social memory. Elife *4*, e03614. https://doi.org/10.7554/eLife.03614.

31. John, S.R., Dagash, W., Mohapatra, A.N., Netser, S., and Wagner, S. (2022). Distinct dynamics of theta and gamma rhythmicity during social interaction suggest differential mode of action in the medial amygdala of sprague dawley rats and C57BL/6J mice. Neuroscience *493*, 69–80. https://doi.org/10.1016/j.neuroscience.2022.04.020.

32. Dulac, C., and Wagner, S. (2006). Genetic analysis of brain circuits underlying

pheromone signaling. Annu. Rev. Genet. *40*, 449–467. https://doi.org/10.1146/annurev.genet.39.073003.093937.

33. Mehta, M.R. (2005). Role of rhythms in facilitating short-term memory. Neuron *45*, 7–9. https://doi.org/10.1016/j.neuron.2004.12.030.

34. Barta, T., and Kostal, L. (2019). The effect of inhibition on rate code efficiency indicators. PLoS Comput. Biol. *15*, e1007545. https://doi.org/10.1371/journal.pcbi.1007545.

35. Ferguson, K.A., and Cardin, J.A. (2020). Mechanisms underlying gain modulation in the cortex. Nat. Rev. Neurosci. *21*, 80–92. https://doi.org/10.1038/s41583-019-0253-y.

36. Gobrogge, K.L., Liu, Y., Jia, X., and Wang, Z. (2007). Anterior hypothalamic neural activation and neurochemical associations with aggression in pair-bonded male prairie voles. J. Comp. Neurol. *502*, 1109–1122. https://doi.org/10.1002/cne.21364.

37. Haller, J., Tóth, M., Halasz, J., and De Boer, S.F. (2006). Patterns of violent aggression-induced brain c-fos expression in male mice selected for aggressiveness. Physiol. Behav. *88*, 173–182. https://doi.org/10.1016/j.physbeh.2006.03.030.

38. Ricci, L.A., Schwartzer, J.J., and Melloni, R.H., Jr. (2009). Alterations in the anterior hypothalamic dopamine system in aggressive adolescent AAS-treated hamsters. Horm. Behav. *55*, 348–355. https://doi.org/10.1016/j.yhbeh.2008.10.011.

39. Reis, F.M., Lee, J.Y., Maesta-Pereira, S., Schuette, P.J., Chakerian, M., Liu, J., La-Vu, M.Q., Tobias, B.C., Ikebara, J.M., Kihara, A.H., et al. (2021). Dorsal periaqueductal gray ensembles represent approach and avoidance states. Elife *10*, e64934. https://doi.org/10.7554/eLife.64934.

40. Hahn, J.D., and Swanson, L.W. (2015). Connections of the juxtaventromedial region of the lateral hypothalamic area in the male rat. Front. Syst. Neurosci. *9*, 66. https://doi.org/10.3389/fnsys.2015.00066.

41. Semenenko, F.M., and Lumb, B.M. (1999). Excitatory projections from the anterior hypothalamus to periaqueductal gray neurons that project to the medulla: a functional anatomical study. Neuroscience *94*, 163–174. https://doi.org/10.1016/s0306-4522(99)00317-6.

42. Vandecasteele, M., Royer, S.M.S., Belluscio, M., Berényi, A., Diba, K., Fujisawa, S., Grosmark, A., Mao, D., Mizuseki, K., et al. (2012). Large-scale recording of neurons by movable silicon probes in behaving rodents. JoVE, e3568. https://doi.org/10.3791/3568.

43. Knobloch, H.S., Charlet, A., Hoffmann, L.C., Eliava, M., Khrulev, S., Cetin, A.H., Osten, P., Schwarz, M.K., Seeburg, P.H., Stoop, R., and Grinevich, V. (2012). Evoked axonal oxytocin release in the central amygdala attenuates fear response. Neuron *73*, 553–566. https://doi.org/10.1016/j.neuron.2011.11.030.

44. Yizhar, O., Fenno, L.E., Davidson, T.J., Mogri, M., and Deisseroth, K. (2011). Optogenetics in neural systems. Neuron *71*, 9–34. https://doi.org/10.1016/j.neuron.2011.06.004.

45. Shusterman, R., Smear, M.C., Koulakov, A.A., and Rinberg, D. (2011). Precise olfactory responses tile the sniff cycle. Nat. Neurosci. *14*, 1039–1044. https://doi.org/10.1038/nn.2877.

STAR★METHODS

KEY RESOURCES TABLE

REAGENT or RESOURCE	SOURCE	IDENTIFIER
Antibodies		
primary antibody against c-Fos, Anti-rabbit	Cell signaling	Cat# 2250S; RRID: AB_2247211
secondary antibody [Alexa fluor 594-conjugatedanti-rabbit IgG antibody	Abcam	Cat # AB-ab150084; RRID: AB_2734147
DAPI + mountant	GBI labs	E19-18
Bacterial and virus strains		
ssAAV-1/2-hSyn1-hChR2(H134R)_mCherry-WPRE-hGHp(A)	Zurich VVF, Switzerland	v124-1
Chemicals, peptides, and recombinant proteins		
electrodes were coated with a dye, DiI −1,1′-Dioctadecyl-3,3,3′,3′-tetramethylindocarbocyanine perchlorate	Invitrogen	D3911
Deposited data		
Mendeley Data, V2, https://doi.org/10.17632/k6htkkfz42.2	Mendelay	
https://doi.org/10.5281/zenodo.7322678	Zenodo	
Experimental models: Organisms/strains		
C57BL/6J mice	Envigo Israel	
BALB/cJ mice	Envigo Israel	
CD-1 (ICR) mice	Envigo Israel	
Software and algorithms		
FlyCapture2	Flir	
Intan Recording Controller Software	Intan	
pClamp9	Molecular Devices	
NIS Elements viewer software	Nikon	
TrackRodent	https://github.com/shainetser/TrackRodent	
MATLAB 2017-2022	MATLAB	
SPSS v23.0	IBM	
Other		
Flea3 USB3 camera	Flir	FL3-U3-13E4M-C
metal grid floor connected to an electrical shock-delivering unit	Coulbourn Instruments	H10-11M And H13-14
Mill-Max female connector	Mill-Max	#853-43-100-10-001000
16 Ni-chrome wires, polyimide insulated, 12 µm diameter core bare at the tip	AM systems	AM-761000
100 µm silver wire	AM systems	AM-785500
miniature custom-made drive	Parts as in - Vandecasteele et al., 2012	
Platinum Black Plating Solution	Neurolynx	26023-84-7
LCR meter	Tonghui	TH2822
RHD2000 evaluation system RHD2132 amplifier ultra-thin SPI interface cable	Intan	

(*Continued on next page*)

Continued

REAGENT or RESOURCE	SOURCE	IDENTIFIER
200 mm optic fibers with 0.39 NA. 10.5 mm ceramic ferrule (outer diameter of 2.5 mm)	Thorlabs	FT200UMT
power meter	Thorlabs	PM100D
glass capillary	BRAND, disposable BLAUBRAND®	708707
laser (473 nm)	Blue Sky Research	model FTEC2471-M75YY0
Master8 Channel Programmable Pulse Stimulator	A.M.P.I	
VT1000s sliding vibratome	Leica	
Ti2 fluorescent microscope	Nikon	
infrared DIC microscope (BX51WI)	Olympus	
Axopatch 200B amplifier and a 1550B digitizer	Molecular Devices	
blue-light led (excitation λ = 450-480 nm)	Prizmatix	

RESOURCE AVAILABILITY

Lead contact

Further information and requests for resources and reagents should be directed to and will be fulfilled by the lead contact, Shlomo Wagner, (shlomow@research.haifa.ac.il).

Materials availability

This study did not generate new unique reagents.

Data and code availability

- The processed datasets analyzed during the current study (Table S3) as well as the detailed statistical analyses (Table S1) and the normality checks of transformed results (Table S2) are deposited in Mendeley Data and available using the following reference - Netser, Shai (2022), "Data and statistical summary for the paper - Modulation of social investigation by anterior hypothalamic nucleus rhythmic neural activity", Mendeley Data, V2: https://doi.org/10.17632/k6htkkfz42.2.
- The raw LFP signals and spike times, time labels of stimuli insertion and removal and the camera frames' time stamps, as well as the results of video analyses by TrackRodent are all uploaded to Zenodo: https://doi.org/10.5281/zenodo.7322678
- All custom-made codes or any additional information required to reanalyze the data reported in this paper is available from the lead contact upon request.

EXPERIMENTAL MODEL AND SUBJECT DETAILS

Animals

Mouse subjects were naive C57BL/6J adult male mice (8-18 weeks old), commercially obtained (Envigo, Israel). Social stimuli were in-house grown C57BL/6J juvenile male mice (3-6 weeks old) in the SP and free interaction tests, or adult male C57BL/6J, BALB/cJ or CD-1 (ICR) mice in the case of the SFC paradigm and SxP, or adult female C57BK\6J for the SxP test. All animals were kept in groups of 2-5 per cage at the animal facility of the University of Haifa under veterinary supervision, in a 12 h light/12 h dark cycle (lights on at 9 p.m.), with *ad libitum* access to food (standard chow diet, Envigo RMS, Israel) and water. In experiments involving electrodes or optic fiber implantation, mice were kept in isolation for about 7 days following surgery.

Institutional review board

All experiments were performed according to the National Institutes of Health guide for the care and use of laboratory animals and approved by the Institutional Animal Care and Use Committee (IACUC) of the University of Haifa.

METHOD DETAILS

Experiments

Behavioral experiments took place during the dark phase of the animals, under dim red light. All experiments were performed according to the National Institutes of Health guide for the care and use of laboratory animals and approved by the Institutional Animal Care and Use Committee (IACUC) of the University of Haifa.

Experimental setups

Social preference and sex preference setup

The experimental setup[25] consisted of a white Plexiglas arena (37 × 22 × 35 cm) placed in the middle of an acoustic chamber (60 × 65 × 80 cm). Two Plexiglas triangular chambers (12 cm isosceles, 35 cm height) were placed in two randomly selected opposite corners of the arena, in which an animal or object (plastic toy) stimulus could be placed. A metal mesh (12 × 6 cm, 1 × 1 cm holes) placed at the bottom of the triangular chamber allowed direct interaction with the stimulus through the mesh. A high-quality monochromatic camera (Flea3 USB3, Flir), equipped with a wide-angle lens, was placed at the top of the acoustic chamber and connected to a computer, enabling a clear view and recording (~30 frames/s) of the subject's behavior using a commercial software (FlyCapture2, FLIR).

Free interaction setup

Following the SP test, the chambers separating the subjects from the social stimuli were removed from the arena, and a free interaction session was conducted in the same arena.

Social fear conditioning setup

The SFC setup was a custom-made white Plexiglas arena similar in size to the experimental setup for the social preference test (37 × 22 × 35 cm) but with a metal grid floor (H10-11M, Coulbourn Instruments) connected to an electrical shock-delivering unit (precision regulated animal shocker H13-14, Coulbourn Instruments). The unit was modified to deliver a single pulse of 0.3-0.4 mA for 750 ms when manually triggered.

Behavioral paradigms

Social preference/free interaction paradigm used for electrophysiology

After connecting the subject to the recording system, it was left for a 15-min habituation to an arena containing empty chambers. Throughout this time, social stimuli were placed in similar chambers near the acoustic chamber for acclimation. The recording session started with an additional 5 min of baseline (pre-encounter) period with the empty chambers. Thereafter, the empty chambers were replaced with chambers containing the social and object (plastic toy, ~5 × 5 cm) stimuli, and the SP test was conducted for 5 min. Following the SP test the stimuli-containing chambers were replaced again with the empty ones for an additional 5 min of recordings (post-encounter, see Figure 1A). Then, the empty chambers were removed from the arena, and the subject was left alone for 20 min. Next, the recording started again for an additional 5 min of baseline (pre-encounter), followed by a 5-min test of free interaction with a novel social stimulus taken directly from its home cage and an additional 5 min of post-encounter period after removal of the social stimulus back to its home-cage. Each subject (n = 17) animal was tested 2-6 times, with at least 6 h between distinct sessions with the same subject.

Social preference and sex preference used for in vivo optogenetic stimulation

In both the SP and SxP tests, subject animals (n = 9 for SP, n = 5 for SxP) were first connected to stimulation apparatus and left for a 20-min habituation to an arena containing empty chambers. The interaction was recorded for 5 min, after replacement of the empty chambers with the social and object stimuli chambers in the SP test, and with the male and female stimuli in the SxP test. In the SP test, each subject was tested three times – unstimulated (Figure 6E), stimulated at the beginning of social investigation bouts (Figure 6F), or stimulated when being near the object - when the animal was in the half part of the arena containing the object chamber (Figure 6G). The three types of experiments were randomly conducted with the same animals, each on a separate day. As for the SxP test, each subject was tested twice - once with optic stimulation delivered at the beginning of investigatory bouts with the female stimulus (Figure 7A), and once with optic stimulation delivered at the beginning of investigatory bouts with the male stimulus (Figure 7B).

Social fear conditioning paradigm

The SFC paradigm consisted of a 15-min habituation of the subjects to an arena containing two empty chambers, followed by two consecutive SP tests with social stimuli of two distinct strains (C57BL/6J and either ICR or BALB/cJ), separated by a 15-min interval. Thereafter, the subject was transferred to the SFC arena for a 15-min habituation, followed by 5 min of the SFC procedure, in which the subject received a mild electrical foot shock (0.3-0.4 mA, 750 ms) each time it tried to interact with the chamber containing the social stimulus (ICR or BALB/cJ strains). Five minutes after conditioning, the subject was returned to the experimental arena for a 15-min habituation and two more consecutive SP tests, as before conditioning (Early recall tests). The animals were then placed back in their home-cages and a day later were returned to the experimental arena for a 15-min habituation, and two more consecutive SP tests were performed (Late recall tests). In sessions with electrophysiological recordings (n = 7), the animal's behavior and brain activity were recorded for 5 min of pre-encounter (with empty chambers), 5 min of encounter (with the social stimulus), and 5 min after the encounter (with empty chambers). In sessions in which the animals were sacrificed for c-Fos immunostaining (n = 14, out of which four from each group were randomly taken for analysis), the Late recall test was done only once, with one of the social stimuli (C57BL/6J or BALB/cJ).

Electrode implantation surgery

Mice were anesthetized and analgized with an intraperitoneal injection of a mixture of ketamine, Domitor, and the painkiller Norocarp (0.13 mg/gr, 0.01 mg/gr, and 0.005 mg/gr, respectively). Anesthesia level was monitored by testing toe pinch reflexes and additional doses (30% of the initial dose) were administered if necessary. The body temperature of the animals was kept constant at approximately 37°C, using a closed-loop custom-made temperature controller connected to a temperature probe and a heating pad placed under the animal. Anesthetized animals were fixed in a stereotaxic apparatus (Kopf Inst.), with the head flat. The skin was then removed, and holes were drilled in the skull for implanting a custom-made tetrode probe, fixing supporting screws (stainless steel, 1.4 mm in diameter, 3 mm long) and placing reference and ground silver wires. The custom-made probe consisted of 4 tetrodes (16 Ni-chrome wires, polyimide insulated, 12 μm diameter core bare at the tip, AM systems) glued to an optic fiber (320 μm with coating, Thorlabs) and fixed to a custom-made 3D plastic-printed scaffold (See Figure S1A). The tip of each wire was inserted to a 9*2 Mill-Max female connector (Interconnect Machined Pin Socket, #853-43-100-10-001000, Mill-Max) stripped of pins, which were then inserted back to the socket by manually pressing them into it. The assembly was then glued on a miniature custom-made drive[42] which enabled driving the probe deeper into the brain between sessions if no spikes were detected. The wires were then plated with Platinum Black Plating Solution (Neurolynx) to lower the impedance down to a range of 200 kΩ to 350 kΩ (measured using LCR meter, Tonghui). The additional two pins were soldered to silver wires (100 μm silver wire, AM systems) and served for reference and ground. Before implantation, electrodes were coated with a dye, DiI (1,1′-Dioctadecyl-3,3,3′,3′-tetramethylindocarbocyanine perchlorate, dissolved in 70% ethyl-alcohol; Invitrogen), for fluorescent marking aimed to track their position postmortem. Tetrodes were implanted above the AHN (A/p = − 0.85 mm, L/M = − 0.2 mm, D/V = − 4.75 mm) and were driven into the AHN before the recording sessions. The drive, wires, and screws were fixed by dental cement and the implant was covered with copper foil plates, which were connected to the ground wire as well.[42] After the surgery, Antisedan was given subcutaneously to wake the mice from the anesthesia. The mice were then placed in a warm cage (37°C) overnight. The animals were injected with Norocarp and Baytril (5%, 0.03 mL/10gr) to relieve pain and prevent infections for three days following the surgery. Behavioral testing and electrophysiological recordings were conducted at least five days post-surgery.

Electrophysiological recordings

Electrophysiological recordings were performed via the RHD2000 evaluation system, using an ultra-thin SPI interface cable and a RHD2132 amplifier board (Intan Technologies). A custom-made Omnetics-to-MillMax adaptor was used to connect between the tetrodes and amplifier.[31] Recorded signals (sampled at 20 kHz) were synchronized with the video recording by a start signal sent through a custom-made triggering device and TTL signals from the camera to the recording system.

In vivo optogenetic stimulation

Optic fiber

To enable *in vivo* delivery of light, optic fibers were prepared in-house by inserting 200 mm optic fibers with 0.39 N A. into a 10.5 mm long ceramic ferrule with outer diameter of 2.5 mm (Thorlabs), gluing them in

place, and polishing the ferrule tip with 30, 6, and 3 μm sandpapers (Thorlabs). The optic fiber tip was then cut to an appropriate length to reach the AHN. Light power at the tips of the fibers was measured for adequate power output (~10 mW) using a power meter (Thorlabs) prior to implantation. This parameter was later used to determine the driving voltage needed for achieving identical stimulation power in all cases.

Surgery for virus injection and optic fiber implantation

Subject mice were first anesthetized as described above. The mouse's head was then shaved and fixed in a stereotaxic apparatus (Kopf Inst.). The scalp was cut to reveal the skull, and measurements were then taken to ensure alignment of the skull. The AHN was targeted according to the coordinates described above for *in vivo* electrophysiology. Once the coordinates were marked, a hole (unilateral, right hemisphere) was drilled, and a glass capillary filled with the virus (ssAAV-1/2-hSyn1-hChR2(H134R)_mCherry-WPRE-hGHp(A), Zurich VVF, Switzerland) was slowly lowered into the target region and left in place for 5 min prior to injection and 10 min following injection to prevent retraction of the virus. A total of 300 nL of the virus was then delivered by manual application of pressure using a 50 mL syringe connected to the glass capillary (BRAND, disposable BLAUBRAND micropipettes, intra-Mark, 5 μl). Following the viral injection, an optic fiber was inserted into the region of interest with the same coordinates as the viral injection, and placed 100 μm above the injection depth. After the surgery, Antisedan (0.1mL/10gr bodyweight) was given subcutaneously to wake the mice from the anesthesia. The mice were then placed in a warm cage (37°C) overnight. The animals were injected with Norocarp and Baytril (5%, 0.03 mL/10gr) to relieve pain and prevent infections for three days following the surgery. Behavioral testing was conducted three weeks after the viral injection.

Optogenetic stimulation

On the day of testing, mice were lightly anesthetized with isoflurane and connected to the laser (473 nm, model FTEC2471-M75YY0, Blue Sky Research) for light delivery. Animals were given 20-30 min to recover from any residual effects of the brief isoflurane anesthesia before testing, until they showed full mobility. Light power was set at 5 mW, which is sufficient to yield 1 mW/mm^2 - the minimum amount of light reported to be capable of efficient ChR2 activation,[43] positioned no farther than 0.25 mm above the AHN. This should lead to a specific stimulation of the AHN, as previous measurements with blue light stimulations in rodent brains have shown that the blue light of the laser does not penetrate the tissue further than 500 μm.[44] Each animal underwent three sessions of SP on separate days as described above. The optical stimulation in all cases was a 1 s train of 20 ms pulses delivered at 20 Hz. These parameters were chosen in accordance with the study of Anthony et al. (2014). The optical stimulation was manually delivered via a Master8 Channel Programmable Pulse Stimulator (A.M.P.I).

Postmortem histological location analysis of electrodes and optic-fibers

Animals were perfused with PBS (PBS) and then fixed using 4% paraformaldehyde (PFA, Sigma) solution. The brains were harvested and placed in PFA (4%) for 48 h, followed by sectioning of 50-μm slices on the horizontal axis using a VT1000s sliding vibratome (Leica.) Sections were stained with DAPI and examined under a wide-field fluorescence microscope (Nikon Ti-eclipse) for verifying the placement of the electrodes' marks (DiI fluorescence) or the optic fiber within the AHN (Figure S1C).

***In vitro* electrophysiology**

Two C57BL/6J adult male mice were injected with the viral vector as described above and kept in their home-cages for 4-8 weeks until their brains were harvested by decapitation following anesthesia with isoflurane. Fresh coronal brain slices (300 μm thick) were obtained in ice-cold oxygenated (95% O_2-5% CO_2) normal saline Ringer solution (in mM: 124 NaCl, 3 KCl, 2 $MgSO_4$, 1.25 NaH_2PO_4, 26 $NaHCO_3$, 2 $CaCl_2$, and 10 glucose). AHN-containing slices were incubated for at least 1 h in room temperature. Then, the slices were transferred to a recording chamber perfused with Ringer solution maintained at 30°C, located beneath an infrared DIC microscope (BX51WI Olympus; Tokyo, Japan), with 10X or 40X water immersion objectives. Neurons expressing mCherry were identified for current-clamp recordings by their red fluorescence using excitation λ = 545-580 nm, emission $\lambda \geq$ 610 nm (fluorescence filter from Olympus, U-MWIY2).

Whole-cell current-clamp recordings were performed to measure the action potential firing rate using an Axopatch 200B amplifier and a 1550B digitizer (Molecular Devices, Sunnyvale, CA). Borosilicate glass

pipettes (3–5 MΩ) were used with a 2-step electrode puller (Narishige PC-10) to make recording electrodes, which were then filled with internal solution (130 mm K-gluconate, 5 mm KCl, 10 mm HEPES, 2.5 mm $MgCl_2$, 0.6 mm EGTA, 4 mm Mg-ATP, 0.4 mm Na_3GTP, and 10 mm phosphocreatine: osmolarity 290 mOsm, pH 7.3). Data were obtained utilizing pClamp9 (Molecular Devices), acquired at 5 kHz and digitized at 2 kHz. Once the neuron was electrically accessible, the voltage data were obtained after the pipette capacitance and series resistance were compensated for manually. Before the recordings started, the blue-light pulse (excitation λ = 450-480 nm, ultra-high power led, Prizmatix) intensity was adjusted between 3 and 5 mW/mm^2 until a single action potential was observed. Once optimized, the same light intensity was maintained throughout the recording of that cell. In order to validate the functionality of the virus *ex vivo*, trains of 20 pulses (pulse duration 1 ms) were delivered at 5 Hz, 10 Hz, 20 Hz, and 40 Hz with a 30-s inter-train interval. Additionally, a train of 20-ms long pulses was delivered at 20 Hz. The light pulse train was delivered both sequentially (each trial containing all the frequencies) and each frequency with repeated trials.

c-Fos expression

Ninety minutes following the Late recall test, mice were transcardially perfused with 100-200 mL of 0.1M PBS (PBS) (pH = 7.4), followed by ~100 mL 4% Paraformaldehyde (PFA) in PBS. The brains were removed and kept in 4% PFA until sectioning. Coronal brain slices of 50 μm thickness were obtained as described above.

Free-floating brain sections were rinsed (3 × 10 min) in PBS and incubated in blocking solution [PBS+5% normal goat serum (Biological Industries) and 0.3% Triton X-100 (Fluka analytical)] for 2 h at room temperature. Then, the sections were incubated with primary antibody against c-Fos [Anti-rabbit (Cell signaling) 1:500] at 4ºc in a shaking incubator overnight. The sections were then rinsed again in PBS (3 × 10 min) and treated with secondary antibody [Alexa fluor 594-conjugatedanti-rabbit IgG antibody (Abcam), 1:500] for 2 h at 4ºc. After washing in PBS (3 × 10 min) at room temperature, sections were mounted on clean glass slides, air-dried, and cover slipped with DAPI + mountant (GBI labs).

Microscopy

Fluorescence images were acquired through a 20X objective lens and a Zyla camera or a 10× objective and a Nikon camera, attached to the Nikon Ti2 fluorescent microscope. The images were acquired using a blue filter for DAPI staining, and TRITC for the c-Fos expressing cells. The image files were visualized using NIS Elements viewer software (Nikon) to manually count c-Fos-stained cells. Number of cells was an average over six randomly selected AHN slices per animal.

QUANTIFICATION AND STATISTICAL ANALYSIS

Tracking software and behavioral analyses

All recorded video clips were analyzed using TrackRodent (https://github.com/shainetser/TrackRodent).[25] For analysis of SP sessions, we used the *BlackMouseWiredBodyBased* algorithm and for free interaction sessions we employed the *BlackMice_TwoMiceFreeInteraction* algorithm as previously described.[31]

Analysis of LFP signals

All signals were analyzed using a custom-made MATLAB program. First, the signals were down-sampled to 5 kHz and low-pass filtered up to 0.3 kHz using a Butterworth filter. The power over time for the different frequencies was constructed by the "spectrogram" function in MATLAB, using a 2 s long discrete prolate spheroidal sequences (DPSS) window with 50% overlap, at 0.5 Hz increments and 0.5 s time bins. The power for each frequency band (Theta: 4-12 Hz and Gamma: 30-80 Hz) was averaged for each recorded channel. The channel chosen for further analysis was the one with the highest and most stable signal to noise ratio (SNR) in the specific frequency (Theta or Gamma) during the post-encounter period (mean divided by SD of the signal).

For evaluation of the change in activity across the entire recording session, the signal was Z-scored by subtraction of the mean power and division by the SD of the pre-encounter period. For presentation, the average *Z* score was calculated in 10 s bins.

Synchronization between the LFP signal and investigation bouts toward social or object stimuli was assessed by calculating the power within a time window of 5 s before and 6 s after the beginning of each

bout (using 1 s bins) and then averaging the responses to all bouts for each session. Thereafter, the mean power was normalized separately for each session using *Z* score analysis, with the 5 s before the bouts serving as a baseline.

Analysis of spiking activity

All signals were analyzed using a custom-made MATLAB program. First, the signals were band-pass filtered from 0.3 kHz to 5 kHz using a Butterworth filter. Then, the time of spikes in each channel was detected using a threshold of 3.5 SD(calculated for each minute of the recording separately). We then sorted the spikes into single and multi-units based on the data from each tetrode using PCA analysis based on the spike shape and amplitude using the software package written by Alexei A Koulakov.[45] Since many of the spikes could not be sorted well into single units, we considered all units as multi-unit activity.

The change in multi-unit activity across the entire recording session and its synchronization with the investigation bouts were analyzed in a similar manner to the LFP analysis. For presentation, the average *Z* score was calculated in 30 s bins.

Spike-triggered LFP (stLFP) analysis

We calculated stLFP by averaging short segments of the LFP signal aligned with each spike. First, raw LFP signals were band-pass filtered at the Theta range and normalized by subtracting the mean and dividing by the SD of the entire signal recorded. Next, short segments of 200 ms, centered around each spike occurring during the encounter, were averaged for each unit separately. In addition, we averaged a similar number of segments around random time points within the encounter time (shuffled-LFP). For statistical comparison between the real and shuffled data, we summed the stLFP and shuffled-LFP average at the time window of −10 to +10 ms around the spike time. It should be noted that more than 1500 spikes were recorded from each multi-unit, therefore no multi-unit was excluded.

Statistical analysis

All results and parameters of the statistical analyses are detailed in Table S1 according to the related figure. Sample size for all experiments was based on previously published power calculations.[25] All statistical tests were performed using SPSS v23.0 (IBM) except for the analysis of covariance, which was performed using MATLAB (using the function " aoctool"). The Kolmogorov-Smirnov test was used for verifying the normal distribution of the dependent variables. When normality was not assumed, Square-Root or Hyperbolic Arcsine transformation was applied to the data to yield normal distribution needed for the application of parametric tests. All normality checks for the transformed results are detailed in Table S2. A two-tailed paired t-test was used to compare between different conditions or stimuli for the same group, and a two-tailed independent t-test was used to compare a single variable between distinct groups. For comparison between multiple groups and parameters, a mixed model (MM) ANOVA was applied to the data. This model contains one random effect (ID), one within effect, one between effect, and the interaction between them. For comparison within a group using multiple variables, a two-way repeated-measures (RM) ANOVA model was applied to data. This model contains one random effect (ID), two within effects, one between effect, and the interactions between them. All ANOVA tests were followed, if main effects or interaction found, by *post hoc* Student's *t* test with Bonferroni correction. When the sphericity assumption needed for ANOVA was violated, Greenhouse-Geisser correction was used. When sample size was smaller than 5, or when normality could not be achieved even after transformation, non-parametric tests were applied. For comparing between multiple independent groups Kruskal-Wallis test was used, followed by Dunn's multiple comparisons for *post hoc* analysis. For comparing between multiple related samples, Friedman's test was used followed by Wilcoxon *post hoc* comparisons. Significance was set at 0.05 and was adjusted using Bonferroni correction when multiple comparisons were used.